J. Fluid Mech. (2013), *vol.* 715, *pp.* 60–102. © Cambridge University Press 2013
doi:10.1017/jfm.2012.498

Turbulence in transient channel flow

S. He† and M. Seddighi

Department of Mechanical Engineering, University of Sheffield, Sheffield S1 3JD, UK

(Received 10 July 2012; revised 20 September 2012; accepted 5 October 2012)

Direct numerical simulations (DNS) are performed of a transient channel flow following a rapid increase of flow rate from an initially turbulent flow. It is shown that a low-Reynolds-number turbulent flow can undergo a process of transition that resembles the laminar–turbulent transition. In response to the rapid increase of flow rate, the flow does not progressively evolve from the initial turbulent structure to a new one, but undergoes a process involving three distinct phases (pre-transition, transition and fully turbulent) that are equivalent to the three regions of the boundary layer bypass transition, namely, the buffeted laminar flow, the intermittent flow and the fully turbulent flow regions. This transient channel flow represents an alternative bypass transition scenario to the free-stream-turbulence (FST) induced transition, whereby the initial flow serving as the disturbance is a low-Reynolds-number turbulent wall shear flow with pre-existing streaky structures. The flow nevertheless undergoes a 'receptivity' process during which the initial structures are modulated by a time-developing boundary layer, forming streaks of apparently specific favourable spacing (of about double the new boundary layer thickness) which are elongated streamwise during the pre-transitional period. The structures are stable and the flow is laminar-like initially; but later in the transitional phase, localized turbulent spots are generated which grow spatially, merge with each other and eventually occupy the entire wall surfaces when the flow becomes fully turbulent. It appears that the presence of the initial turbulent structures does not promote early transition when compared with boundary layer transition of similar FST intensity. New turbulent structures first appear at high wavenumbers extending into a lower-wavenumber spectrum later as turbulent spots grow and join together. In line with the transient energy growth theory, the maximum turbulent kinetic energy in the pre-transitional phase grows linearly but only in terms of u', whilst v' and w' remain essentially unchanged. The energy production and dissipation rates are very low at this stage despite the high level of u'. The pressure–strain term remains unchanged at that time, but increases rapidly later during transition along with the generation of turbulent spots, hence providing an unambiguous measure for the onset of transition.

Key words: pipe flow boundary layer, turbulent flows, turbulent transition

1. Introduction

1.1. *Motivation and scope*

Unsteady flow is frequently encountered in engineering applications as well as the natural environment, including for example, power plant start-up or shut down, the

† Email address for correspondence: s.he@sheffield.ac.uk

https://doi.org/10.1017/jfm.2012.498 Published online by Cambridge University Press

sudden closure of valves in a pipeline system, passenger trains going through a railway tunnel, the blood flow in the human body and waves over the beach. A better understanding and improved prediction of unsteady flow have remained a strong drive for investigations into various forms of unsteady flows to improve the safety, economy and comfort of engineering systems and for the preservation of the environment. In addition to practical applications, unsteady turbulent flow has also been an intriguing topic of fundamental turbulence research since it reveals flow physics that is not always apparent in steady flows. Consequently, unsteady flow has remained a subject of continuing investigation. The particular motivation of our work has originated from the need for accurate prediction of wall shear stresses in unsteady flows encountered in studies of sediment transport under sea waves (Van *et al.* 2011) and the development of methodologies for leak detection (Colombo, Lee & Karney 2009).

This paper reports a new study on the response of turbulence in a transient channel flow based on direct numerical simulations (DNS) of a Poiseuille flow in a parallel-plane channel of infinite spanwise dimension. The flow is initially steady turbulent at a relatively low flow rate, but it is suddenly increased to and kept at a much higher value and we study the transient behaviour of the flow in response to this change. It is shown that the flow response bears striking similarity to the boundary layer bypass transition to turbulence induced by free-stream turbulence (FST). The flow structures of elongated streamwise streaks and the generation of isolated turbulent spots that are characteristic of the laminar–turbulent transition are observed to prevail in this transient turbulent flow, which is demonstrated by the instantaneous flow and supported by analysis of the ensemble-averaged flow statistics.

The finding is fundamental because it suggests that a low-Reynolds-number turbulent flow can undergo a process of transition that resembles the laminar–turbulent transition. As the flow rate of the turbulent channel flow is rapidly increased, the new flow is re-established as a result of this transition, rather than progressively developing from the initial turbulent flow. This new understanding also leads to new interpretation of the statistics of transient flows. The results reported herein could have profound implications for the understanding and prediction of many unsteady flows encountered in practice, and could lead to the development of new strategies for turbulence control, all of which are yet to be explored.

The specific objectives of the paper are: (i) to illustrate the transient channel flow transition phenomenon by studying the instantaneous flow and compare it with observations in boundary layer bypass transition; (ii) to establish that the transient channel flow is dominated by a time-developing boundary layer initially formed on the wall in response to the rapid change of flow rate and compare its characteristics with those of the external boundary layer, including the thickness, shape factor and friction coefficient; (iii) to study the energy growth, streak characteristics, turbulence generation mechanisms and receptivity and compare them with experimental and computational results of boundary layer bypass transition, and hence to establish the similarities and differences between the two flows; and (iv) to re-interpret unsteady flow data in view of this transition.

To lay the background for discussion, the remaining part of the Introduction is devoted to a summary of previous investigations of unsteady channel and pipe flows followed by a brief review of recent developments in the study of transition with a focus on boundary layer bypass transition.

https://doi.org/10.1017/jfm.2012.498 Published online by Cambridge University Press

1.2. *Studies on unsteady flows*

A detailed study of transient flow in a pipe was conducted in the 1970s by Maruyama, Kuribayashi & Mizushina (1976) who performed an experimental investigation into turbulence responses following a step increase or decrease of flow rate from an initially turbulent flow. The stepwise variation of the flow rate was achieved by suddenly opening or closing one of two identical valves placed in parallel, with which flow rates in the main circuit could be doubled or halved within a fraction of a second. The diameter of the pipe was 51 mm and the low and high Reynolds numbers were 5000 and 10 000 respectively. The distribution of the axial velocity in the fluid and the velocity gradient on the wall were measured using an electrochemical method. Ensemble-averaged mean velocity and the turbulent fluctuating velocity were obtained from repeated runs of the same unsteady flows. By studying the variation of turbulence intensity, it was concluded that the generation and propagation of new turbulence is the dominant process in the step-increase case and the decay of the old turbulence in the step-decrease case. The propagation time is determined by the condition at its generation. In addition, it was concluded that the dynamic processes in both cases are governed by the same essential mechanisms, that is, the stepwise change of the generation of the turbulence corresponding to the final steady flow and the so-called temporal coherence of its propagation in the radial direction.

The study of He & Jackson (2000) was concerned with a linearly accelerating and decelerating flow from an initially steady turbulent flow using a two-component laser Doppler anemometer (LDA). In contrast with Maruyama *et al.* (1976)'s experiments, the acceleration was maintained at a constant rate during the period of the measurement, which was varied systematically. The experiments were carried out with water in a pipe of diameter of 50.8 mm with the Reynolds number varying between 7000 and 42 000. The two-component LDA was used to produce measurements of all three velocity components by first conducting simultaneous measurements of u and v, and then u and w at a specific time. Ensemble-averaged mean velocity, and all three components of the normal stresses as well as the shear stresses were obtained from many repeated identical unsteady flow experiments. The responses of turbulence were explained by associating them with turbulence production, turbulence energy redistribution and the radial propagation of turbulence. At any location, turbulence shows a two-stage response: an initial slower response (referred to as a delay stage) and a faster response which brings it close to the steady value rapidly. The study confirmed the findings of Maruyama *et al.* (1976) that turbulence first responds in the near-wall region and then propagates towards the centre of the pipe. It further showed that in the buffer region the axial component of turbulence responds earlier than the other two components, whereas in the core, the three components behave in a similar manner.

Greenblatt & Moss (2004) focused on a higher starting Reynolds number and relatively faster accelerations. The experiments were carried out in a pipe of 48 mm in diameter with water as the working fluid and a one-component LDA was used to measure the instantaneous velocity. The flow was rapidly increased from a Reynolds number of 31 000 to 82 000 within 0.85, 1.62 and 3 s in three test cases. In each case, the acceleration rate was fast and nearly constant in the first half-period, but was much slower and gradually diminishing in the second half-period. In essence, the first half of the test is similar to that of He & Jackson (2000) where the flow is subjected to a roughly constant acceleration, whereas in the later stage, the flow undergoes relaxation in response to an increase of flow rate occurred earlier resembling that of

https://doi.org/10.1017/jfm.2012.498 Published online by Cambridge University Press

Maruyama *et al.* (1976). Consistently with He & Jackson and Maruyama *et al.*, the authors found that in a rapidly accelerating flow, turbulence is initially frozen everywhere, but then starts to increase first close to wall, and gradually propagating to other regions. In contrast with early studies, however, a second peak of turbulence response was found in a region further away from the wall at around $y^+ = 300$. This phenomenon was not fully understood and was hypothetically associated with the higher starting Reynolds number that was used in the study and hence not observed in earlier studies.

He, Ariyaratne & Vardy (2011) carried out an experimental study of wall shear stress in an accelerating flow of water in a pipe of a large diameter (100 mm) using flush-mounted hot-film sensors. The wall shear stress was shown to follow a three-stage development. In Stage 1, it initially increases rapidly overshooting the pseudo-steady value, but then increases more slowly and eventually falls below the pseudo-steady value. In Stage 2, it increases rapidly again, and finally in Stage 3 approaches and fluctuates around the quasi-steady values. Such behaviour of the wall shear was related to turbulence responses in the core previously identified in the studies discussed above. Stage 1 was associated with a period of minimal turbulence response when the turbulent wall shear stress remains largely unchanged except for a very slow increase which was hypothetically associated with the stretching of existing turbulent eddies as a result of flow acceleration. At the condition of nearly 'frozen' turbulence, the unsteady wall shear stress is driven primarily by flow inertia. The start of Stage 2 was associated with the generation of new turbulence causing both the mean and turbulent wall shear stress to increase rapidly. The turbulent wall shear, reflecting local turbulent activities near the wall, responds first and the mean wall shear, reflecting conditions across the entire flow field, responds somewhat later. The duration of the initial period of nearly frozen turbulence response increases with decreasing initial Reynolds number and increasing acceleration. The latter is in contrast with the response of turbulence in the core of the flow, which has been shown by He & Jackson (2000) to be independent of the rate of acceleration.

Chung (2005) performed a DNS of unsteady turbulent channel flow subjected to a sudden decrease in the pressure gradient at low Reynolds numbers ($Re_\tau = 240$–360). Overall, the characteristics of the flow were similar to those of quasi-steady flow since the prescribed rate of change of the pressure gradient was small. Seddighi *et al.* (2011) carried out a similar DNS study to that of Chung but with much stronger deceleration rates and included an accelerating flow in the same Reynolds number range. In the strongly decelerating flow, turbulence response exhibits a two-stage development, initially remaining 'frozen' for a period before reducing. The responses of the three components of the r.m.s. of the fluctuating velocities in the ramp-up and -down flows were compared directly. In a ramp-up flow, more energy is in the axial component and less in the other two, but this is reversed in a ramp-down flow.

Pulsating flows over a mean turbulent flow with relatively small amplitude and oscillating flows crossing the zero-flow-rate condition are also interesting unsteady flows that have been studied extensively recently. Much of the flow physics of such flows are common to that of the ramp-type flow studied herein. However, comparison between the various flows is beyond the scope of this paper and hence no review of the studies on pulsating or oscillating flows is provided here. Interested readers are referred to the recent studies including, for example, Scotti & Piomelli (2001), Tardu & Da Costa (2005) and He & Jackson (2009) for pulsating flows and Fornarelli & Vittori (2009) and Van *et al.* (2011) for oscillating flows.

https://doi.org/10.1017/jfm.2012.498 Published online by Cambridge University Press

1.3. *Studies of transition to turbulence*

Transition to turbulence has remained a classical research topic in fluid mechanics for over a century since the publication of Osborne Reynolds' landmark experiment (Reynolds 1883). The fundamental physics in various flow configurations, such as a pipe, a channel and an external boundary layer, is largely the same but the detailed transition mechanisms vary from flow to flow. Linear stability analysis has shown that pipe flow is stable for very high Reynolds numbers in response to infinitesimal perturbations; for example, Meseguer & Trefethen (2003) analysed the problem up to $Re = 10^7$. However, in practice, the flow may become turbulent at a Reynolds number of $\sim$2300 and above as demonstrated in the classical Reynolds experiment. On the other hand, when the experimental conditions are carefully controlled to have very small external disturbances, the flow may remain laminar for up to a Reynolds number of 10^5 (Pfenninger 1961). The early stage of transition is characterized by the generation of turbulent spots which expand to fill the entire cross-section of the pipe in one of two forms: namely, puffs or slugs (Wygnanski & Champagne 1973; Shan *et al.* 1999). Puffs occur for Reynolds numbers within the range of 1750–2700 when perturbations trigger the generation of intermittent turbulent spots which coexist with the laminar flow. For higher Reynolds numbers, the turbulent spots are much larger in size occupying a longer section of the pipe, which are referred to as slugs. The mechanism of transition is still a current issue intriguing both theoreticians as well as practitioners. Very recently, much research has focused on the transient nature of turbulence and the key factors that keep turbulence sustained, examples of which include Mellibovsky *et al.* (2009) and Avila *et al.* (2011). Systematic reviews of recent theoretical and experimental studies on transition in a pipe can be found in Eckhardt *et al.* (2007), Willis *et al.* (2008) and Mullin (2011).

Transition to turbulence in plane Poiseuille channel flow is predicted to occur at a Reynolds number of 5772, based on the centreline velocity and the channel half-height, by Orszag (1971) through directly solving the Orr–Sommerfeld equation numerically. In reality, both experiments and DNS have shown that transition is likely to occur at a Reynolds number of 1000 or slightly above which is referred to as subcritical transition. The generation of turbulent spots and their spread are most important characteristics of the transition which have been studied both experimentally and computationally (e.g. Carlson, Windall & Peeters 1982; Schumacher & Eckhardt 2001; Lagha 2007). Turbulent spots typically extend the full height of the channel and spread many channel heights spanwise. A spot may be initiated closer to one of the walls but is also affected by the opposite wall. This is due to the nature of the confined flow at relatively low Reynolds numbers. Only with a very high Reynolds number of 8000, did Zang & Krist (1989) find that turbulent spots are generated and remain close to one wall with limited effect from the opposite wall.

Linear instability analysis of external boundary layer flow has yielded the Tollmein–Schlichting-wave-induced transition to turbulence which is a very slow process that occurs at a high Reynolds number of the order of $Re_x = 10^6$. When the free-stream turbulence is in the order of 1 % or more, however, transition is observed to occur at Reynolds numbers of an order of magnitude lower and at a much faster rate, bypassing the Tollmein–Schlichting instability, which is consequently known as the bypass transition.

Typically bypass transition takes place in three regions (Jacobs & Durbin 2001), i.e. a buffeted laminar boundary layer, isolated turbulent spots and the fully turbulent boundary layer. In the first region, large perturbations from the free-stream turbulence penetrate into the laminar boundary layer, which are then amplified to produce

https://doi.org/10.1017/jfm.2012.498 Published online by Cambridge University Press

elongated streaks of faster and slower axial velocities. These streaks remain largely stable at this stage. Towards the end of the first region, the flow reaches a condition such that local instability starts to occur at isolated locations, which eventually evolves into patches of turbulent spots. These spots grow both longitudinally and spanwise, occupying more and more space until they fill the full span of the flow field when the flow becomes fully turbulent.

Bypass transition is an extremely complex phenomenon. Despite being a subject of intensive studies, there are still many open issues. No attempt is made here to provide a complete review of research on bypass transition; instead, a brief review of some more recent studies is given below to facilitate the discussion of the results on transient channel flow. The readers are referred to the review of Durbin & Wu (2007) and more recent papers of original studies, such as, Mandal, Venkatakrishnan & Dey (2010) and Nolan, Walsh & McEligot (2010) for further information.

Klebanoff (1971) made a useful contribution in identifying streaks of positive and negative axial velocity perturbations in the early stages of bypass transition and showed that these 'narrow spanwise disturbances' spread roughly linearly with the boundary layer thickness. Such streamwise streaks have been widely accepted as a major feature of the early stage of bypass transition, which are now known as Klebanoff modes although these are not really modes in the sense of being eigenfunctions. Matsubara & Alfredsson (2001) used flow visualization to show the presence of the streaky structures, which have a well-defined spanwise scale. Some of those streaks were witnessed to break down into turbulent spots, and subsequently grow into other areas until the boundary layer is fully turbulent. Fransson *et al.* (2005) performed further experiments focusing on the effect of FST intensity and scale as well as modelling of the transition zone. They showed that the disturbance energy grows linearly with the Reynolds number based on the downstream distance, and that the transitional Reynolds number is inversely proportional to the initial FST squared. Asai, Minagawa & Nishioka (2002) experimentally investigated the growth and breakdown of a single low-speed streak in a boundary layer, which was produced using a small piece of screen set normal to the wall. They were able to reproduce and study both the antisymmetric sinuous and symmetric varicose modes of transition. Based on a series of experimental and DNS studies of bypass transition, Schlatter *et al.* (2008) further elucidated the two different mechanisms of streaky structures prior to turbulent spot generation, noting that the sinuous mode occurs much more often than the varicose mode. More recent experiments of Mandal *et al.* (2010) and Nolan *et al.* (2010) produced further evidence of the streaky structures in bypass transition: while the former focused on a proper orthogonal decomposition (POD) analysis of the fluctuating velocity field, the latter used quadrant analysis.

Following early DNS studies of bypass transition by Rai & Moin (1993) and Voke & Yang (1995), Jacobs & Durbin (2001) reported a well-resolved DNS of FST-included transition with the turbulent inflow constructed using Orr–Sommerfeld continuous modes. This method enabled them to employ a rather fine mesh in a reduced computational domain that did not include the leading edge. They identified long backward jets contained in the fluctuating axial velocity flowing backwards relative to the local mean velocity as the key features of the transition. These jets appear to have resulted from the penetration of low-frequency free-stream disturbances. They sometimes extend into the upper portion of the boundary layer where they interact with free-stream eddies. Turbulent spots are believed to result from such interactions. Using a method similar to that used by Jacobs & Durbin (2001), Brandt, Schlatter & Henningson (2004) performed DNS to study the effect of FST with

https://doi.org/10.1017/jfm.2012.498 Published online by Cambridge University Press

variable length scales and intensities, and found that increasing either of them causes the transition to move upstream. They discussed the two types of low-speed streak breakdown scenarios, namely the sinuous mode and the varicose mode, and this was reinforced in Schlatter *et al.* (2008) mentioned above.

Nagarajan, Lele & Ferziger (2007) studied the bypass transition with blunt/sharp super-elliptical leading edges using large-eddy simulation (LES). For a sharp leading edge with low FST, they observed transition via streak breakdown similar to those observed by Brandt *et al.* (2004); but for a blunt leading edge and/or a high FST, a different transition mechanism was identified which is characterized by localized wavepacket-like oscillations in the spanwise velocity. These are initially generated by stretching the free-stream vortices before the formation of well-defined streaks. Such wavepackets were found to have different characteristics from the spot precursors observed in the cases of streak breakdown. Ovchinnikov, Choudhari & Piomelli (2008) performed DNS of bypass transition due to high-amplitude FST for a flat plate using a domain beginning upstream of the leading edge. The length scale of the FST was found to have a significant influence on the transition mechanism: when the length scale is small, the streamwise streaks (Klebanoff modes) were seen to be the dominating instability, whereas for large-scale FST cases, instability came from the wavepacket-type oscillations discussed in Nagarajan *et al.* (2007). However, the precursors were found to stem from spanwise structures in the wall-normal component rather than in the streamwise vertical structures. Wu & Moin (2009) also conducted a DNS of boundary layer flow over a flat plate with intermittent localized disturbances arising from patches of turbulence (5 %) introduced at $Re_\theta = 80$. The study focused on producing reliable flow statistics for fully developed turbulence although transition was also studied. The results showed that the nonlinear dynamical development of Λ-shaped vortices into hairpin packets is responsible for the breakdown of the Blasius layer and streaks are generated alongside this process.

Theoretical studies have been carried out by Andersson, Berggren & Henningson (1999) and Luchini (2000) to investigate the characteristics of disturbances on transient growth and have identified the so-called optimal disturbance that causes the maximum growth rate. Zaki & Durbin (2005) combined a theoretical study with computational simulations to investigate the manner by which external disturbances penetrate into the laminar boundary layer and induce transition. Coupled continuous spectrum Orr–Sommerfeld and Squire modes were used to characterize the disturbances. The complete transition process was captured with one low-frequency mode together with one high-frequency mode. The findings of this work are supported by Hernon, Walsh & McEligot (2007)'s experimental investigation and are further extended in the theoretical work of Zaki & Saha (2009), both of which also studied the 'shear sheltering' phenomenon. Ricco, Luo & Wu (2011) investigated the influence of unsteady free-stream disturbances modelled using convected gusts consisting of a pair of oblique modes of the same frequency but opposite spanwise wavenumbers. With such a simple model, they were able to reproduce the key features of transition observed in experiments (Matsubara & Alfredsson 2001) and DNS (Jacobs & Durbin 2001). Vaughan & Zaki (2011)'s theoretical work investigated the secondary instability of a boundary layer due to unsteady streaks using Floquet analysis, which was complemented with DNS. Two most unstable modes were identified which were referred to as the inner and the outer instability, respectively, for cases whose critical layers occur at the outer edge of the boundary layer or close to the wall. They related these to the two types of transition mechanisms observed in the literature, namely the Klebanoff modes dominating in the results of Jacobs & Durbin (2001) and Brandt

https://doi.org/10.1017/jfm.2012.498 Published online by Cambridge University Press

et al. (2004) and the wavepacket-type instability observed by Nagarajan *et al.* (2007) and Ovchinnikov *et al.* (2008). The authors reported growth rates for these different types of instabilities for a range of frequencies and amplitudes of the base streaks, and hence identified a critical amplitude. For the Klebanoff modes, the critical amplitude required by the varicose mode was found to be much greater than that of the sinuous mode, which is consistent with Schlatter *et al.* (2008)'s observation that the latter occurs more often than the former.

In summary, pipe flow is a unique case where the flow is theoretically predicted to be stable at a very high Reynolds number (say, up to 10^7) in response to infinitesimally small disturbances, but becomes turbulence at a low Reynolds number of $\sim$2300 in practice when finite disturbances are present. Transition occurs in the form of either puffs or slugs. The transitional Reynolds number for a plane Poiseuille flow is predicted to be 5772 by linear stability analysis, but in practice transition may occur at a much earlier stage due to the influence of finite disturbances. Studies have focused on formation and growth of turbulent spots which often occupy the full height of the channel and many channel heights spanwise. Most studies of pipe and channel flows are for relatively small Reynolds numbers and turbulent spots fill the entire cross-section in the case of a pipe or are confined by the two walls in the case of a plane channel. Boundary layer transition occurs at $\sim Re_x = 10^6$ due to Tollmien–Schlichting waves, but again transition may occur at a much lower Reynolds number when the free-stream turbulence is greater than 1 % (bypass transition). The study reported in this paper shows that the transient channel flow behaves strikingly similarly to the boundary layer bypass transition. Unlike the typical transition scenarios of the confined flows (pipe or channel flow) at low Reynolds numbers, the processes over the two walls are independent to each other.

2. Methodology

Direct numerical simulations of transient turbulent channel flow are performed using an 'in-house' code (Seddighi 2011; Seddighi *et al.* 2011) solving a dimensionless form of the momentum and continuity equations as follows:

$$\frac{\partial u_i}{\partial t} + u_j \frac{\partial u_i}{\partial x_j} = -\frac{\partial p}{\partial x_i} + \frac{1}{Re}\nabla^2 u_i, \tag{2.1}$$

$$\frac{\partial u_i}{\partial x_i} = 0, \tag{2.2}$$

where $i, j = 1, 2, 3$ stand for the streamwise, wall-normal and spanwise directions respectively. The length, velocity, time and pressure are normalized with the channel half-height (δ), a characteristic velocity (U), a time scale (δ/U) and ρU^2, respectively, where ρ denotes the density, and $Re = U\delta/\nu$, where ν denotes viscosity. In the simulations, the centreline velocity of the laminar Poiseuille flow at the initial flow rate is used as the characteristic velocity. However, for ease of explanation of the results and comparison with data from the literature, the results presented in this paper are re-scaled using the bulk velocity of the final flow (U_{b1}) as the characteristic velocity.

Equations (2.1) and (2.2) are discretized on a rectangular staggered mesh with a non-uniform distribution in the wall-normal direction and a uniform distribution along the other two directions. The spatial derivatives are discretized using a second-order central finite-difference method. An explicit low-storage, third-order Runge–Kutta scheme is used for the temporal discretization of the nonlinear terms and a second-

https://doi.org/10.1017/jfm.2012.498 Published online by Cambridge University Press

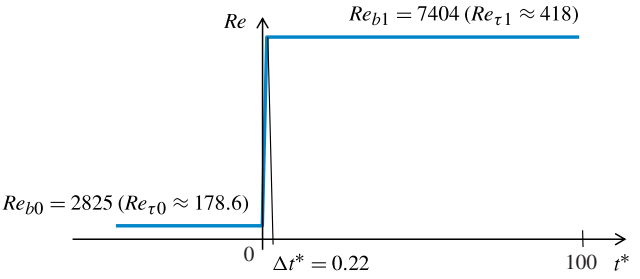


FIGURE 1. (Colour online) The prescribed flow variation; $t^* = t/(\delta/U_{b1})$.

order implicit Crank–Nicholson scheme for the viscous terms. These are combined with the fractional-step method to enforce the continuity constraint (Kim & Moin 1985; Orlandi 2001). In this method, each time advancement consists of three steps and in each step, the discretized equations are first solved for an intermediate non-solenoidal velocity field without a full consideration of the continuity constraint. The Poisson equation is then solved for a virtual pressure field which is subsequently used to project the velocity field onto a solenoidal velocity field. Finally, the message-passing interface (MPI) is used to parallelize the code for use on a distributed-memory computer cluster. More detailed information on the numerical methods used in the 'in-house' DNS code is given in the Appendix.

The computational domain for the channel flow is 12.8δ, 2δ and 3.5δ in the streamwise, wall-normal and spanwise directions, respectively. The suitability of this domain is discussed later. Periodic boundary conditions are applied to the streamwise and spanwise directions and non-slip boundary conditions are applied to the top and bottom walls. Figure 1 shows the variation of the flow simulated. The simulations of the transient flow begin from an initially fully developed steady turbulent flow at $Re_b = U_b\delta/\nu = 2825$, where U_b is the bulk velocity. At time $t^*(=t/(\delta/U_{b1})) = 0$, the mass flow rate is increased linearly to $Re_b = 7404$ within a very short period of time ($t^* = 0.22$), and the simulation continues well beyond the time when the flow has again become fully developed ($t^* = 100$). We have adopted a constant-mass-flow condition (as opposed to constant wall shear) in the simulations presented herein. To initiate the acceleration, an addition source term is added to the streamwise pressure gradient at $t^* = 0$, the detail of which is given in the Appendix. The increase of the flow can be treated as a step-change since the acceleration is completed within a very short period of time during which little change is expected to occur in the flow. Note that the acceleration time ($t^* = 0.22$) can be compared with the Kolmogorov and integral time scales of the final flow which are about $t^* = 0.1$ and 0.9, respectively, and the period during which the flow is transient which is about $t^* = 42$ as will be shown later. The corresponding initial and final Reynolds numbers based on friction velocity (U_τ) and half-height ($Re_\tau = U_\tau\delta/\nu$) are 178.6 and 418, respectively. It is worth noting that the initial flow, although commonly known as in the turbulent regime (e.g. Elsnab *et al.* 2011), is at a rather low Reynolds number and some of the observations discussed herein may be specific to such flows. The simulations are repeated 10 times to facilitate the calculations of flow statistics using ensemble averaging. The initial flows for the various runs are taken from different time instants of the same steady flow simulation with a big interval (well above 10 times the integral time) between them to ensure the flow fields are independent of each other.

https://doi.org/10.1017/jfm.2012.498 Published online by Cambridge University Press

	Case	Re_b	Re_τ	Δx^+	Δz^+	Δy^+_{min}	Δy^+_{max}	LX/δ	LZ/δ
Present	Initial flow	2825	178.6	4.47	3.13	0.32	2.96	12.8	3.5
	Final flow	7404	418	10.45	7.3	0.76	6.95	12.8	3.5
Moser *et al.* (1999)	MKM180	2800	178.12	9.7	4.8	0.05	4.4	4π	$\frac{4}{3}\pi$
Abe *et al.* (2001)	AKM395	6990.5	395	9.88	4.94	0.2	9.64	6.4	3.2

TABLE 1. Details of the computational domain and the mesh used in the present study and comparison with simulations from the literature.

The ensemble-averaged statistical quantities for any location a distance y_1 from the wall are obtained through averaging over the plane of $y = y_1$ as well as using repeated runs. Thus the local mean velocity is

$$\overline{u}_s = \frac{1}{MNL}\left(\sum_{k=1}^{L}\sum_{j=1}^{N}\sum_{i=1}^{M} u_s\right) \tag{2.3}$$

and the r.m.s. of the turbulent fluctuating velocity is

$$u'_{s,rms} = \sqrt{\frac{1}{MNL}\left(\sum_{k=1}^{L}\sum_{j=1}^{N}\sum_{i=1}^{M} (u_s - \overline{u}_s)^2\right)}, \tag{2.4}$$

where M and N are the numbers of data points in the streamwise and spanwise directions, respectively, L is the number of repeated runs, $s = 1, 2, 3$ stands for the streamwise, wall-normal and spanwise velocity components, which are also denoted u, v and w. For the plane channel flow studied herein, $\overline{u}$ is the mean streamwise velocity and $\overline{v} = \overline{w} = 0$ for the wall-normal and spanwise directions. The perturbation velocities $u' = (u - \overline{u})$, $v' = v$ and $w' = w$ are referred to as fluctuating velocities.

Both the low and high Reynolds numbers of the transient flow need to be considered when deciding the domain and mesh sizes. The lower Reynolds-number flow requires a relatively larger domain whereas the higher Reynolds-number flow poses a more stringent requirement on the mesh size. Taking all the factors into consideration, the computational domain for the main simulations has been chosen to be $12.8\delta, 2\delta$ and 3.5δ with a mesh of $512 \times 190 \times 200$ in the streamwise (x), normal (y), and spanwise (z) directions respectively. A summary of the key parameters of the simulations is tabulated in table 1, together with information on the simulations of Moser, Kim & Mansour (1999) and Abe, Kawamura & Matsuo (2001), which are chosen as benchmark data for comparison. They provide DNS results for Reynolds numbers close to the initial and final flows of the present study respectively; and the former reproduces the simulations of Kim, Moin & Moser (1987), which are widely used as benchmark data for turbulence study and validation purposes. It is noted that Moser *et al.* (1999) used the spectral approach and, for the same resolution, the results are more accurate than those using finite difference. As a rule of thumb, second-order finite-difference schemes require about twice the resolution to achieve the same results as a spectral DNS (Moin & Mahesh 1998). In the present study, the spatial resolutions in terms of y^+ ($=U_\tau y/\nu$) values are different for the initial and the final flows, both of which are shown. Generally speaking, the spatial resolution based on the initial flow condition is better than that of the benchmark cases but is about the same or

https://doi.org/10.1017/jfm.2012.498 Published online by Cambridge University Press

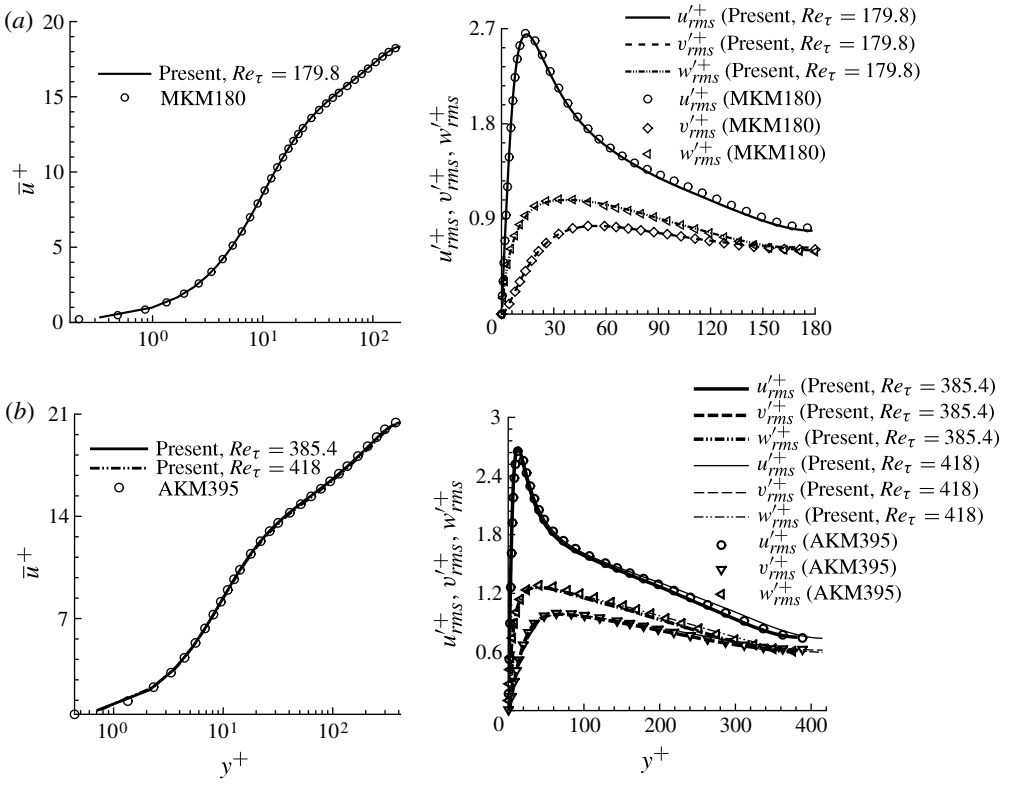


FIGURE 2. Comparison of simulations of steady channel flows with Moser *et al.* (1999) (denoted by MKM180 for $Re_\tau = 178.12$) and Abe *et al.* (2001) (denoted by AKM395 for $Re_\tau = 395$): (*a*) $Re_\tau \approx 180$; (*b*) $Re_\tau = 385$ and 418.

marginally worse than the references based on the final flow condition. For validation purposes including demonstrating the adequacy of the mesh adopted, steady flow results at Reynolds numbers $Re_\tau = 179.8$ ($\sim$ initial flow), $Re_\tau = 385.4$ and $Re_\tau = 418$ (final flow) are compared with the DNS results for similar Reynolds numbers of Moser *et al.* (1999) and those of Abe *et al.* (2001) in figure 2. It is clear that the results of the present study are in excellent agreement with the benchmark data for Reynolds numbers $Re_\tau = 179.8$ and 385.4. It is also clear that the results are only slightly different in the core of the flow when the Reynolds numbers are different (385.4 versus 418), showing weak Reynolds number effects which are expected for low-Reynolds-number flows.

The flow structures in unsteady flows may deviate significantly from those of steady flows and it is necessary to perform additional checks on the adequacy of the computational domain used. Two-point correlations are often used for such a purpose. An important criterion in deciding the computational domain dimension is to ensure the correlation approaches zero within the half-width of the domain. Such a check was performed and it confirms the adequacy of the computational domain used in the present study. The limiting factor is the streamwise velocity correlation R_{11} in the flow direction. The values approach zero well within the half-width for the initial and final steady flows. At certain time instants during the flow transient, the correlation R_{11} increases significantly, but still approaching zero within the half-domain limit, showing

https://doi.org/10.1017/jfm.2012.498 Published online by Cambridge University Press

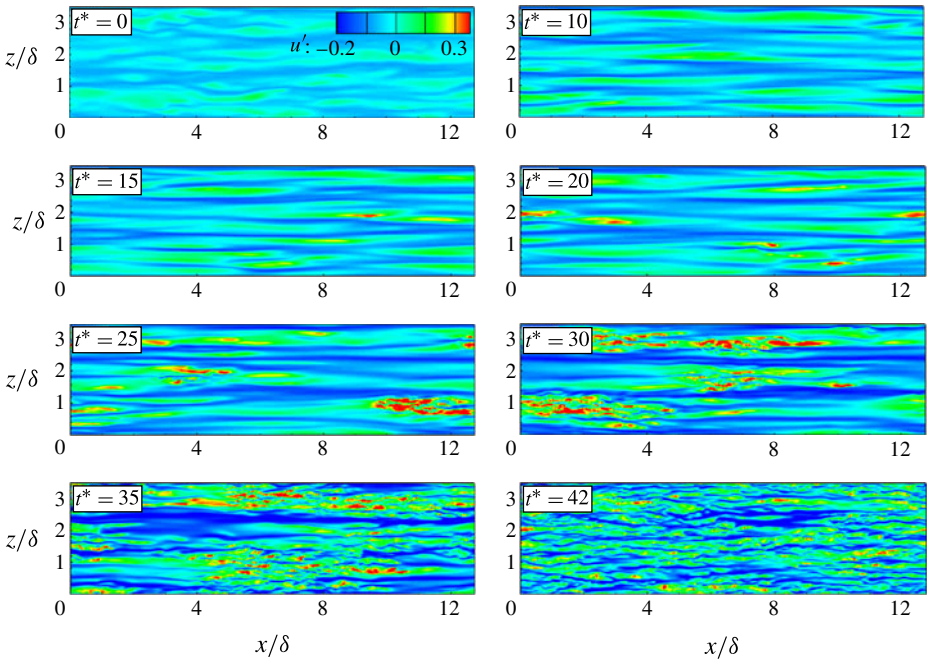


FIGURE 3. Time sequence of contour plots of streamwise fluctuating velocity (u'/U_{b1}) in a plane adjacent to the bottom wall ($y^{+0} = 5.3$).

the adequacy of the size of the computational domain adopted. The transient behaviour of R_{11} is discussed in § 3.2.

3. Results and discussion

3.1. *Instantaneous flow*

Figure 3 shows the contours of the axial component of the fluctuating velocity at $y^{+0} = 5.3$ (where $y^{+0} = U_{\tau_0} y/\nu$ and U_{τ_0} is the friction velocity of the initial steady flow) adjacent to the bottom wall at various times following the rapid increase of flow rate. The values are normalized using the bulk velocity of the final flow, namely $u'/U_{b1} = (u - \overline{u})/U_{b1}$, where u and $\overline{u}$ are the instantaneous and ensemble-averaged velocity, respectively, and U_{b1} the bulk velocity of the final flow. The first frame ($t^* = 0$) corresponds to the steady flow field immediately before the commencement of the transient. Here u' is low and the colour is rather faint, but relatively weak and short patches of high- and low-velocity patterns are clearly seen to exist. In the early stages of the transient (up to about $t^* < 15$), elongated steaks of positive and negative u' have developed which become stronger with time. At around $t^* = 20$, some high fluctuating velocities appear at localized positions, which is followed by observation of the generation of turbulent spots. Initially these spots are fairly localized, but gradually spread to other parts of the flow and merge with each other. Eventually the entire surface is occupied by turbulence ($t^* \sim 42$).

The development of the contours of the fluctuating axial velocity (u'/U_{b1}) described above together with many other characteristics of the flow to be discussed next shows that the response of turbulence in the transient flow under consideration is not a progressive process of development from one turbulent flow condition to another, but

https://doi.org/10.1017/jfm.2012.498 Published online by Cambridge University Press

a process that is strikingly similar to the boundary layer bypass transition observed by many researchers as discussed in the Introduction (e.g. Jacobs & Durbin 2001; Brandt *et al.* 2004; Wu & Moin 2009). The pre-existing turbulence in the flow acts as initial disturbances with respect to the new flow much like the free-stream turbulence in a boundary layer bypass transition. It remains largely unaffected initially by the increased flow rate except close to the wall where such initial turbulence is modulated by a time-developing boundary layer, initially formed adjacent to the wall, but progressively expanding towards the core. As a result, the initial near-wall turbulence structures are stretched to form long 'bubbles' as observed above in the form of elongated streaks in the u' contours. The flow appears to be stable initially and the development of the flow is progressive in nature. At some point in time, the boundary layer develops to a state where some of the streaks break up alongside the generation of turbulent spots. Similar to boundary layer bypass transition, the transient channel flow transition manifests itself initially as the generation of local turbulent packets randomly distributed in space, which grow and connect to each other with time and eventually cover the entire plane. This process takes a considerable period of time, in figure 3 being over the period of $20 < t^* < 42$. In the flow direction, turbulence shows an intermittent feature as turbulent spots travel with the flow. The spots grow in both streamwise and spanwise directions and connect to each other forming large patches of turbulence; but for much of the transitional period, regions of alternating turbulent and 'quasi-laminar' streaky structures coexist. The transitions on the opposite walls are independent of each other. This feature is different from the typical subcritical transition of channel flow at low Reynolds numbers where turbulent spots always occupy the entire channel height (Carlson *et al.* 1982; Lagha 2007).

Another way of visualizing the transition is to inspect the time variation of the velocity at fixed locations. To do this, figure 4 shows the normalized fluctuating velocities u'/U_{b1}, v'/U_{b1} and w'/U_{b1} at several locations along the lines of $z/\delta = 0.9$ (line A) and 2.3 (line B) in the plane of $y^{+0} = 5.3$, respectively. Line A is chosen to be along the locations where turbulent spots are first detected, and the fluctuating velocities clearly show that transition occurs earlier. In addition, the fluctuations show an intermittent feature at the early stage of the transition, reflecting the passing of isolated turbulent spots. At locations along line B, the flow remains 'quasi-laminar' for a longer period of time. The behaviour of u' is clearly different from that of v' and w' before the transition begins (say, about $t^* < 35$ for line B). During this period, u' oscillates slowly but with fairly high amplitudes whereas v' and w' appear to remain laminar-like. The low-frequency oscillations of u' are not related to new turbulence generation but are a reflection of the elongated streaks shown in figure 3 as a result of the stretching of turbulent structures pre-existing in the flow. It is worth noting that turbulent fluctuations in all velocity components largely remain and the 'laminar-like' behaviour of v' and w' is simply due to the scale of plots used to accommodate the final flow. This is clearly demonstrated in figure 4(*c*) which shows the turbulent fluctuating velocity at location a1 before and after the commencement of the transient with a smaller scale. The quantitative behaviours will be discussed later with respect to the r.m.s. of the fluctuating velocities.

The velocity vector plot is a useful tool for identifying the processes of turbulent spot generation in transitional flows. Figure 5 shows the development of the fluctuating velocity fields on a vertical plane at several time instants during the flow transient. To improve the readability of the plots, every other data point in the wall-normal direction and every 16 data points in the flow direction are plotted. Figure 5(*a*) ($t^* = 0$) shows an instant of the steady flow just before the commencement of the

https://doi.org/10.1017/jfm.2012.498 Published online by Cambridge University Press

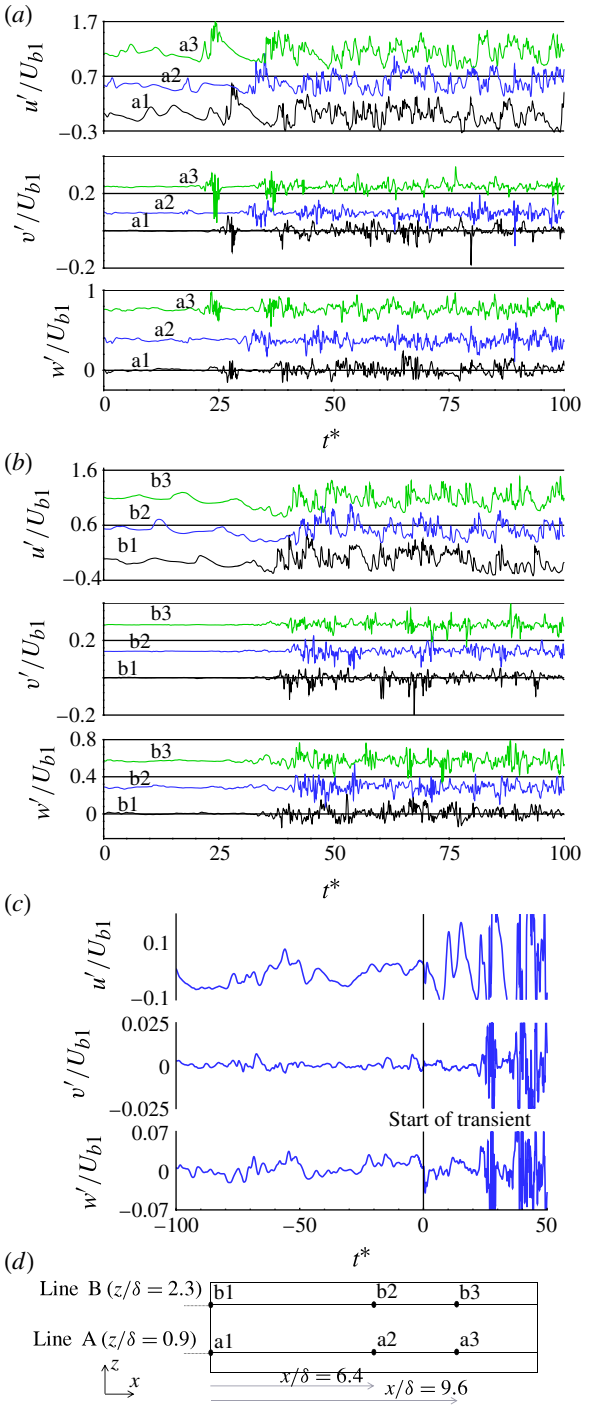


FIGURE 4. (Colour online) Time history of the fluctuating velocities (u', v' and w') during the flow transient at several locations in a plane adjacent to the bottom wall ($y^{+0} = 5.3$): (*a*) line A ($z/\delta = 0.9$); (*b*) line B ($z/\delta = 2.3$); (*c*) pre-transient and initial response at a1 (zoomed-in); (*d*) locations of data presented.

https://doi.org/10.1017/jfm.2012.498 Published online by Cambridge University Press

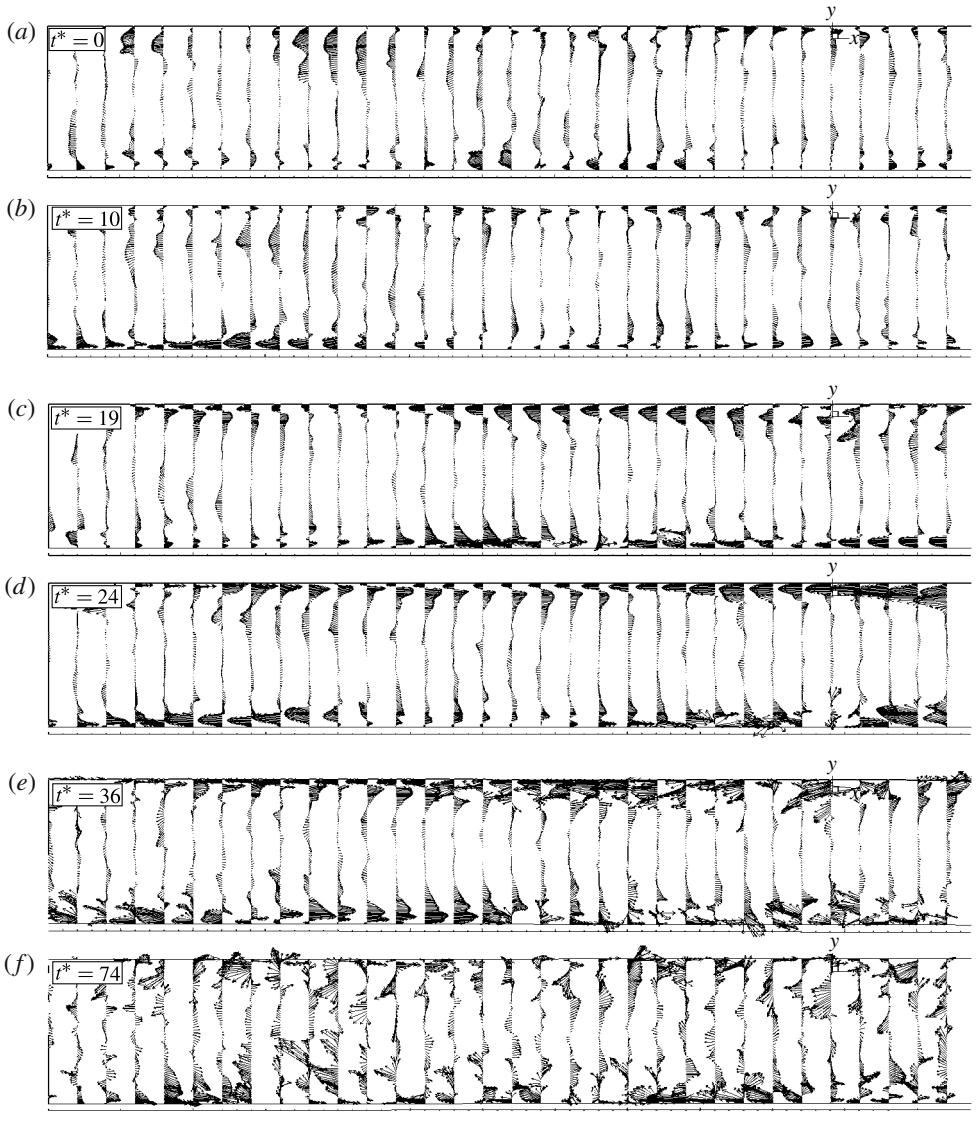


FIGURE 5. Vector plots of fluctuating velocities at several instants in an x–y plane ($z/\delta = 0.9$).

excursion; figure 5(b) ($t^* = 10$) corresponds to pre-transition; figure 5(c) ($t^* = 19$) is around the onset of the transition; figures 5(d) and 5(e) ($t^* = 24$ and 36) correspond to the transition and the last frame ($t^* = 42$) corresponds to the fully turbulent regime. Backward and forward jets in the wall layer are identified in boundary layer transition in both DNS (Jacobs & Durbin 2001; Ovchinnikov *et al.* 2008) and experimental studies (Mandal *et al.* 2010; Nolan *et al.* 2010). These jets manifest themselves as negative and positive velocities in the vector plots, which are often linked to ejection and sweep respectively. It is worth emphasizing that the axial fluctuating velocity u' is the perturbation over the ensemble-averaged local mean velocities, and the backward and forward jets simply represent a deficit and a surplus over the mean velocity

https://doi.org/10.1017/jfm.2012.498 Published online by Cambridge University Press

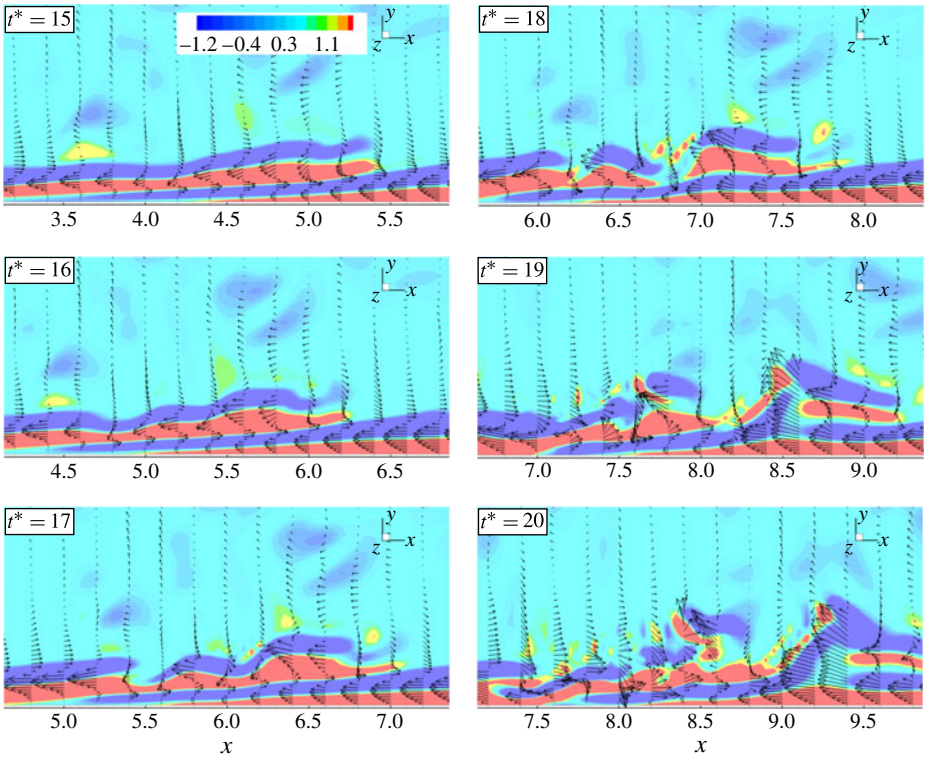


FIGURE 6. Time sequence of contours of the spanwise vorticity (ω_z) and velocity vectors showing the generation of a turbulent spot ($z/\delta = 0.9$).

profile, respectively. Numerous backward and forward jets can be identified in the present results as shown in figure 5. In addition, there are regions where forward jets overlay a backward jet or vice versa. Most of these jets are not directly linked to the initial generation of turbulent spots but some appear to be. This is consistent with observations in boundary layer transitions.

The formation of turbulent spots can be studied by tracing their development backwards with time. As an example, we have identified a turbulent spot at the mid-section of the bottom wall in figure 5(*c*) at $t^* = 19$. Figure 6 shows a zoomed-in window of this section together with several instants before and one after this time, with the location of the window moving with time to follow the structure. Also shown in the figure are contours of the spanwise vorticity (ω_z), with positive values in red and negative in dark blue. At $t^* = 15$, the dominant structure in the boundary layer is a negative jet sitting on top of a positive one, with strong positive vorticity in the middle layer and layers of negative vorticity above and below it. There are also clearly identifiable structures in the main-stream flow. At the next instant ($t^* = 16$), the outlines of the strong-vorticity layers become wavy, and it is stronger in the top layer, suggesting that the source is originated from the main-stream flow. At $t^* = 17$, the wavy structures are much stronger and the top negative-vorticity layer is partly broken. At the same time, the negative-velocity jet streak is also broken. The next few frames show that the disturbances become more violent with time and a turbulent spot is formed. This process is similar to those identified in some

https://doi.org/10.1017/jfm.2012.498 Published online by Cambridge University Press

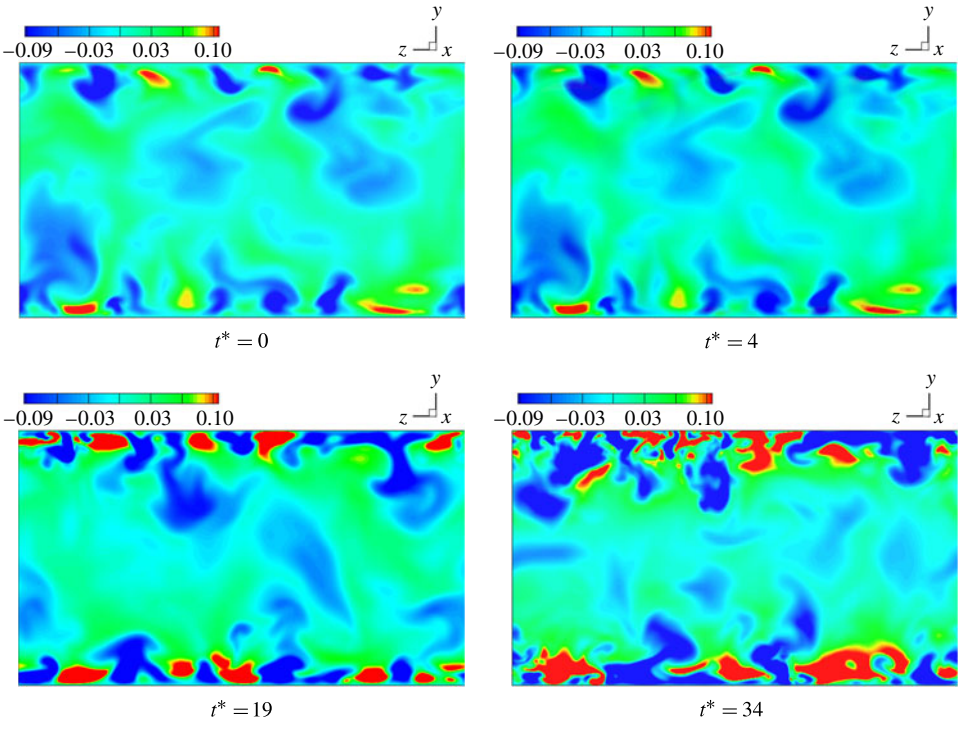


FIGURE 7. Time sequence of streamwise fluctuating velocity (u'/U_{b1}) on a y–z cross-section ($x/\delta = 2.34$).

experimental and computational investigations of boundary layer bypass transitions (e.g. Jacobs & Durbin 2001; Nolan *et al.* 2010). A feature of this process is that the breaking-up appears to always occur near the outer edge of the wall layer where an inflection in velocity is formed as a result of the backward jet. This process is related to Kelvin–Helmholtz instability by some researchers, e.g. Wu *et al.* (1999), Jacobs & Durbin (2001) and Zaki & Durbin (2005, 2006), and is referred to as the outer instability mode by Vaughan & Zaki (2011). It should be noted however that the flow structures are highly three-dimensional and the pictures identified from a two-dimensional plot such as the one discussed above involve some subjective judgments by the researchers. In fact in many cases, the process is very complex and it is difficult to identify any pattern. In this respect, three-dimensional plots such as that presented later in figure 8 give a more comprehensive picture. It is clear though that the turbulent spots seem to be largely associated with backward jets when they are first generated (which is more clearly shown in figure 8). Comparing the flow structures in the top and bottom wall layers (figure 5), it can again be concluded that the transition processes in the two wall layers are independent from each other.

Figure 7 shows a cross-sectional view of the u'/U_{b1} contours at several time instants. The positive velocities of u' are shown in red and the negative velocities are in dark blue. The cross-sectional distribution of the high- and low-axial-velocity streaks, and the extent to which they penetrate into the core of the flow are clearly shown in the figure. The high-speed streaks tend to stay close to the wall, which is understandable because they are mostly associated with wall-normal velocities directed towards the

https://doi.org/10.1017/jfm.2012.498 Published online by Cambridge University Press

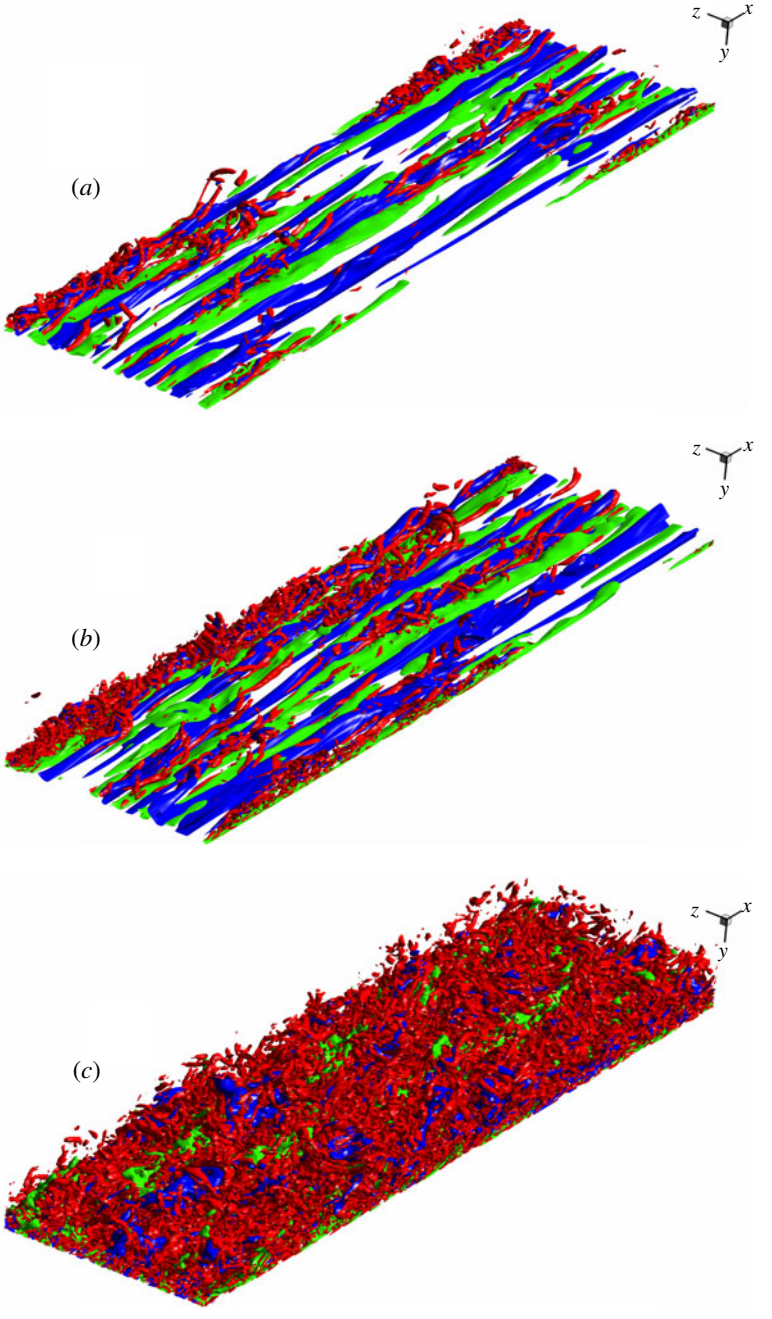


FIGURE 8. Three-dimensional visualization of streaks and vortex structures at instants in: (*a*) the late pre-transitional phase, $t^* = 19$; (*b*) early transitional phase, $t^* = 24$; and (*c*) fully turbulent phase, $t^* = 74$ (iso-surfaces: blue for $u'/U_{b1} = -0.12$, green for $u'/U_{b1} = 0.12$ and red for $\lambda_2 = -0.5$).

wall, which bring high-velocity streams to low-velocity boundary layers. On the other hand, low-speed streaks are frequently seen detached from the wall, and can penetrate

https://doi.org/10.1017/jfm.2012.498 Published online by Cambridge University Press

deep into the core of the flow. This shows that the backward jets may be lifted up from the wall, moving beyond the wall boundary layer and interacting with the core of the flow.

Figure 8 shows three-dimensional iso-surface plots of $u'/U_{b1} = \pm 0.12$ and $\lambda_2 = -0.5$ at a late stage of the pre-transitional phase, an early stage of transition and when the flow is fully turbulent. Here λ_2 is the second largest eigenvalue of the symmetric tensor $\boldsymbol{S}^2 + \boldsymbol{\Omega}^2$ where $\boldsymbol{S}$ and $\boldsymbol{\Omega}$ are the symmetric and antisymmetric parts of the velocity gradient tensor $\nabla \boldsymbol{u}$. This parameter has been demonstrated to be able to effectively identify vortex cores by Jeong & Hussain (1995), and has since been used frequently in studies of transition and turbulence. It can be seen from the figure that at the late pre-transitional stage (and before), iso-surfaces of $u'/U_{b1} = \pm 0.12$ form long tubes which appear alternately, providing further evidence of the streaks identified in figure 3. These iso-surface tubes break up alongside the generation of turbulent spots as transition progresses. Hairpin vortical structures are clearly identifiable through the iso-surface of λ_2. There are fewer such structures in the early pre-transitional stage but many start to appear from the late pre-transition and transition stages. The structures are large and easy to identify initially but towards the late stage of transition and the turbulent stage, the flow field is filled with countless much smaller structures. The vortices often occur around the low-speed streaks accompanying their breakup, which is similar to what is shown in boundary layer transition by Schlatter *et al.* (2008). The formation of vortices throughout the pre-transitional, the transitional and the fully turbulent periods also show close similarity to the vortex development in a boundary layer shown in Wu & Moin (2009).

3.2. *Ensemble-averaged flow field*

In this section, we consider the quantitative behaviour of the transient flow by studying the ensemble-averaged flow statistics and relate them to the visual observations discussed above. The statistics of unsteady flows can be obtained from ensemble averaging results from many repeated unsteady runs, or, based on the ergodic hypothesis, they can also be obtained from averaging the flow over the homogeneous directions, that is, the spanwise and streamwise directions in this study. For the results reported herein, a mixture of the two is used, that is, both the spatial distribution and 10 repeated runs are used for the ensemble average.

A useful place to start is the friction coefficient (C_f), whose transient development reflects the overall response of the flow structure (figure 9). When $t^* \leqslant 0$, the friction coefficient takes a value corresponding to the turbulent flow at $Re_b = 2825$. It increases rapidly to a much higher value during the short period of flow acceleration of $\Delta t^* = 0.22$. It then reduces quickly, reaching a minimum at around $t^* = 20$, before recovering to a value close to that of the final Reynolds number at around $t^* = 42$, after which it remains more or less constant. These two time points ($t^* = 20$ and 42) correspond roughly to the instants when turbulent spots are first observed and when the entire wall region is filled with newly generated turbulent structures, respectively, as seen in figure 3, and are referred to as the start (onset) and the end of the transition herein. The general trend of C_f described above is similar to that observed in the boundary layer bypass transition and a direct comparison with benchmark data will be made below for a modified form of friction coefficient.

3.2.1. *The time-developing boundary layer*

Similarly to the external boundary layer flow, the transient channel flow is also dominated by the evolution of a boundary layer formed on the wall, but one which

https://doi.org/10.1017/jfm.2012.498 Published online by Cambridge University Press

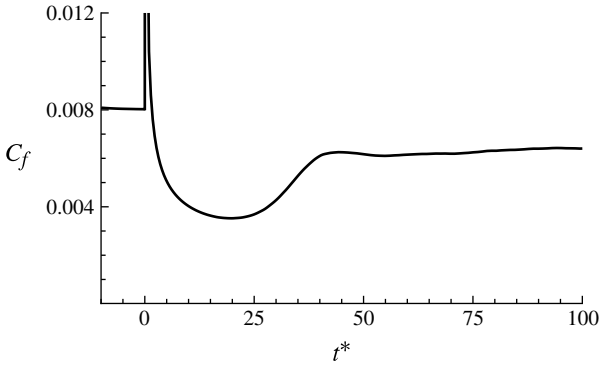


FIGURE 9. Variation of friction coefficient in the transient channel flow.

is uniform in the flow direction but develops outwards with time. As the flow rate is suddenly increased in a channel, the flow initially responds as a solid body everywhere (because the pressure gradient causing the acceleration is uniform on the cross-section of the channel) except for the region very close to the wall due to the no-slip boundary condition. Consequently, the initial perturbation is a very thin layer of high strain rate formed in a region close to the wall, which grows into the flow with time. This time-developing boundary layer is the main source of the change of flow structures to follow, resembling the spatially developing external boundary layer. It is useful to establish a quantitative description of this boundary layer before studying other flow statistics. To this end, we consider the change of the flow by subtracting the initial flow from the transient flow field and normalizing it with its centreline value, namely

$$\overline{u}\hat{}(y/\delta, t^*) = \frac{\overline{u}(y/\delta, t^*) - \overline{u}(y/\delta, 0)}{\overline{u}_c(t^*) - \overline{u}_c(0)} \tag{3.1}$$

where $\overline{u}_c$ is the centreline velocity.

Figure 10 shows the development of the profile of this differential velocity $\overline{u}\hat{}(y/\delta, t^*)$ with time alongside that of the full flow field. The formation of the thin boundary layer on the wall at the beginning of the transient and its growth with time described above qualitatively are now clearly illustrated in figure 10(*a*). The (differential) velocity profile remains flat in the core of the flow, which in this case means that the actual velocity profile remains unchanged from its initial shape. This time-developing boundary layer is directly comparable to the external boundary layer. To further demonstrate this, the data are re-presented against a dimensionless parameter $\eta = y/\sqrt{\nu t}$ in figure 10(*b*). This parameter originates from the non-dimensional parameter $\eta = \sqrt{(u_\infty/\nu x)}y$ used in the Blasius solution, which is rewritten for the time-developing boundary by assuming $U_\infty \sim \overline{u}_c$ and $x \sim t$. For a laminar boundary layer, the profiles of the normalized velocity (u/U_∞) at any downstream location plotted against $\eta = \sqrt{(u_\infty/\nu x)}y$ collapse on top of each other on a single curve given by the Blasius solution. It can be seen that the profiles of the transient flow in the pre-transitional period ($t^* < 20$) indeed collapse reasonably well, indicating that the development of the differential boundary layer resembles that of a laminar flow during this period. It also implies that the growth of the thickness of the boundary layer is proportional to $\sqrt{t}$, resembling the growth rate of $\sqrt{x}$ of an external boundary layer. During the following transitional period, the velocity profile changes quickly, from the Blasius-like profile to one representing a typical turbulent

https://doi.org/10.1017/jfm.2012.498 Published online by Cambridge University Press

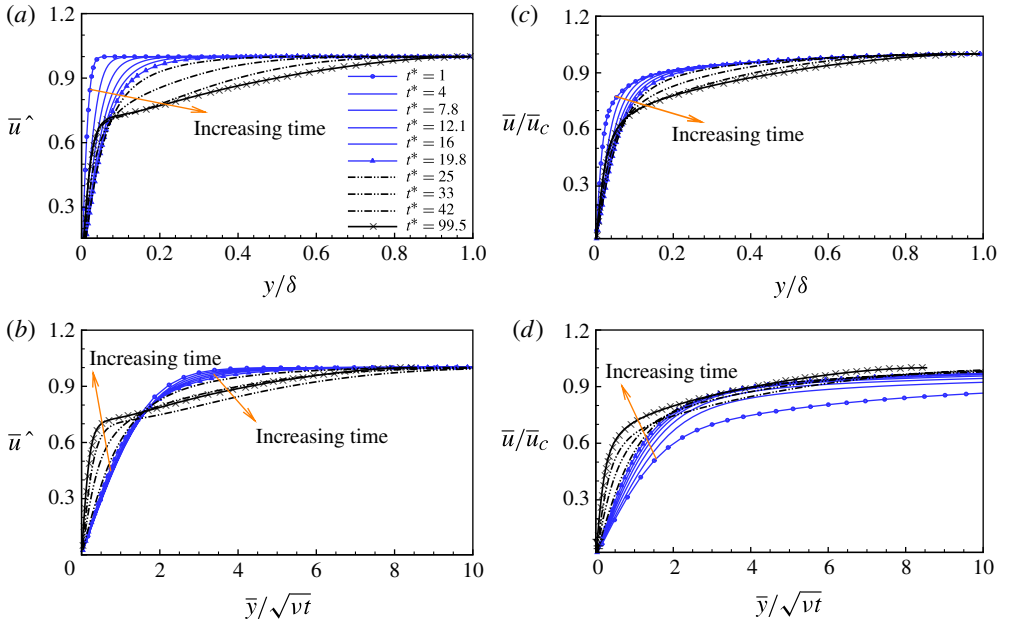


FIGURE 10. (Colour online) Development of the profiles of the differential velocity ($\overline{u}\hat{}$) (*a*,*b*) and the full field velocity ($\overline{u}$) (*c*,*d*) in terms of y/δ in (*a*,*c*) and $y/\sqrt{\nu t}$ in (*b*,*d*).

flow. Figure 10(*c*) shows the development of the full field velocity and figure 10(*d*) shows the normalized form of the full field velocity. The latter does not show good correlation.

Following boundary layer theory, we define the displacement thickness, the momentum thickness and the shape factor of the differential-flow boundary layer at a time t^* as follows:

$$\delta_{du}(t^*) = \int_0^1 (1 - \overline{u}\hat{}(y/\delta, t^*))\mathrm{d}(y/\delta), \tag{3.2}$$

$$\theta(t^*) = \int_0^1 \overline{u}\hat{}(y/\delta, t^*)(1 - \overline{u}\hat{}(y/\delta, t^*))\mathrm{d}(y/\delta), \tag{3.3}$$

$$H(t^*) = \delta_{du}(t^*)/\theta(t^*). \tag{3.4}$$

We further define a friction coefficient based on the differential flow field as

$$C_{f,du} = \frac{\tau_{w,du}}{\frac{1}{2}\rho U_{b1}^2} \tag{3.5}$$

where $\tau_{w,du} = \{\mu\partial[u(y/\delta, t^*) - u(y/\delta, 0)]/\partial y\}|_{y/\delta=0}$. Figure 11 shows the development of the friction coefficient, the Reynolds number based on the momentum boundary layer thicknesses, $Re_\theta = \theta\overline{u}_c/\nu$, and the shape factor during the flow transient. Also shown are experimental results of cases T3A and T3B of Roach & Brierley (1992) for boundary layer bypass transition, and the friction coefficient due to the Blasius laminar boundary layer solution. In order to plot these data on the same figure, a connection between the time of the transient channel flow and the streamwise distance or Re_x of the boundary layer flow needs to be established, which can be done by defining a

https://doi.org/10.1017/jfm.2012.498 Published online by Cambridge University Press

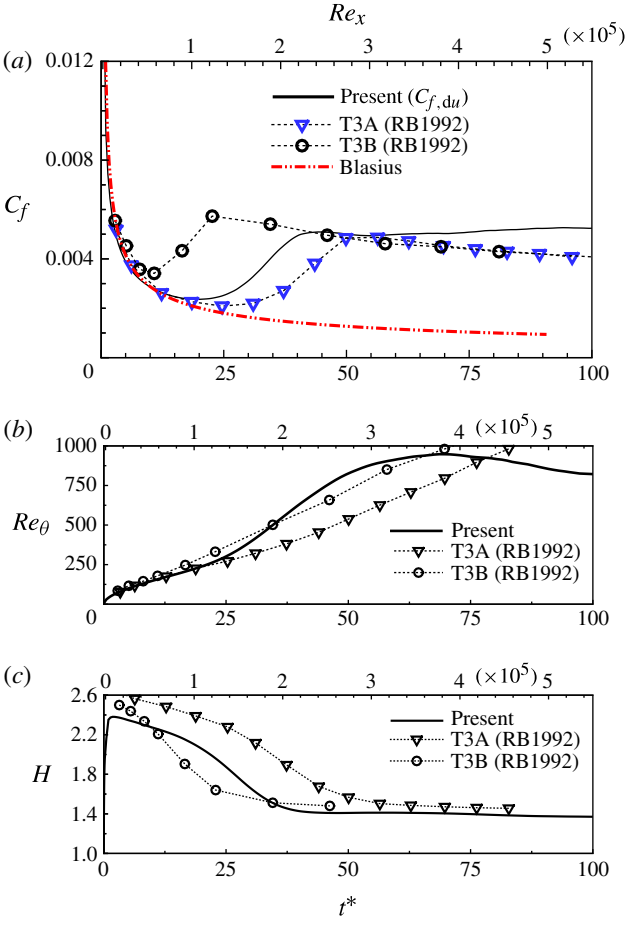


FIGURE 11. (Colour online) Development of the friction coefficient, momentum-thickness Reynolds number Re_θ and shape factor based on the differential flow, and comparison with experimental data of boundary layer transition from Roach & Brierley (1992) (RB1992), and the friction coefficient due to the Blasius solution for a laminar boundary layer.

convective velocity (U_{conv}). This velocity is determined here by best-fitting the Blasius solution with the early response of the transient flow, which gives $U_{conv} = 0.74U_{b1}$.

The experimental results of Roach & Brierley (1992) have been used as benchmark data for FST-induced boundary layer bypass transition by many researchers including, for example, Jacobs & Durbin (2001) and Ovchinnikov *et al.* (2008). The initial FST at the leading edge is 3 % and 6 % for T3A and T3B, respectively, but decays rapidly with the downstream distance. In comparison, the turbulence intensity of the present flow is ∼4 % at the peak wall-normal location ($y^{+0} = 15$) reducing to ∼1.5 % at the centre of the channel, but remaining largely constant with time. It can be seen that similar to the boundary layer bypass transition, the value of $C_{f,du}$ in the transient flow follows the Blasius laminar boundary solution rather closely at the beginning of the transient, only deviating from it slightly approaching the start of the transition. The point of onset of transition in the present study is slightly earlier than that of T3A, but much later than that of T3B. It may not necessarily be appropriate to directly compare the peak turbulence intensity of the channel flow with the FST intensity of

https://doi.org/10.1017/jfm.2012.498 Published online by Cambridge University Press

the boundary layer; nevertheless it is interesting to see that the effect of turbulence intensity appears to be similar in the two flows.

Another factor to consider is the characteristics of the FST, especially the length scale. Through numerical simulations, Ovchinnikov *et al.* (2008) found that the length scale has a profound influence on the transition mechanism although the value of the transitional Reynolds number is only marginally influenced. In the case of FST with a larger integral length scale ($Re_L = UL_{11}/\nu = 6580$, where L_{11} is an integral length scale defined as $L_{11} = \int_0^\infty \overline{u'(x)u'(x+r)}/\overline{u'(x)u'(x)}\,\mathrm{d}r$), the mechanism was found to be due to the formation of turbulent spots upstream of the transition region, whereas the transition of the case with a smaller length scale FST ($Re_L = 1081$) is closely related to the streamwise streak dynamics. The FST in most experimental and numerical studies on boundary layer transition is characterized by a dominant length scale defined by the size of the grid and is fairly homogeneous and isotropic. In the present flow, the initial flow which serves the same purpose as the FST in boundary layer flows is fundamentally different, being a typical low-Reynolds-number wall shear flow with a broad spectrum of turbulence and strong anisotropy. The Reynolds number based on the largest integral length scale (L_{11}) and U_{b1} is $\sim$1300, which is close to the smaller length scale case of Ovchinnikov *et al.* (2008). Consequently, the fact that the generation of turbulent spots is also found to be largely associated with streaks (see for example figure 8) seems to agree with the observations of Ovchinnikov *et al.* (2008) notwithstanding the differences identified above between wall shear turbulence and grid-generated isotropic and homogeneous turbulence.

It can be seen from figure 11(*b*) that the initial development of the momentum thickness is characteristic of a laminar flow, being of quadratic-function shape and agreeing well with that of T3A. During the transition ($20 < t^* < 42$), the slope is significantly increased, much more than that of either set of experimental data. It levels off eventually as the boundary layer reaches the centre of the channel. The transition occurs at $Re_\theta \sim 250$, in line with that of T3A but greater than that of T3B which is less than 200. The trend of the variation of the shape factor in the channel flow is again similar to that of T3A (figure 11*c*), but the magnitude is much lower. Owing to an early transition, the shape factor of T3B is again noticeably different. At the onset of transition, the value of H is $\sim$2 in the transient flow, lower than that in the experimental boundary layer.

3.2.2. *Evolution of the energy of the fluctuating velocities*

An important feature of FST-induced bypass transition is the linear growth of the disturbances in the boundary layer in the direction away from the leading edge before the onset of transition, which is associated with the formation and elongation of streamwise streaks of small spanwise wavenumber. This is consistent with the transient growth theory and has been observed in both experimental and computational studies of bypass transition (e.g. Matsubara & Alfredsson 2001; Brandt *et al.* 2004; Ovchinnikov *et al.* 2008). Figure 12 shows the time development of the maximum values of the three turbulent components as well as the total turbulent kinetic energy, $k = (u'^2_{rms} + v'^2_{rms} + w'^2_{rms})/2$. Note that $2k$ is shown in the figure so that it can be directly compared with u'_{rms}. Both $(u'_{rms}/U_{b1})^2_{max}$ and $(2k/U^2_{b1})_{max}$ show a clear linear increase during the pre-transitional period, after a brief delay. A delay has also been observed in the initial stage of boundary layer flows and is attributed to the adjustment of the disturbances to form the initial streaks. Data on the evolution of the spanwise and the wall-normal components are rarely reported in the literature, but the present

https://doi.org/10.1017/jfm.2012.498 Published online by Cambridge University Press

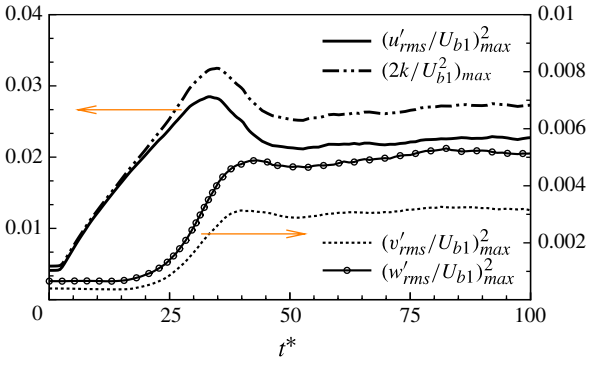


FIGURE 12. (Colour online) Energy growth in terms of peak turbulent kinetic energy and its three components in non-dimensional form.

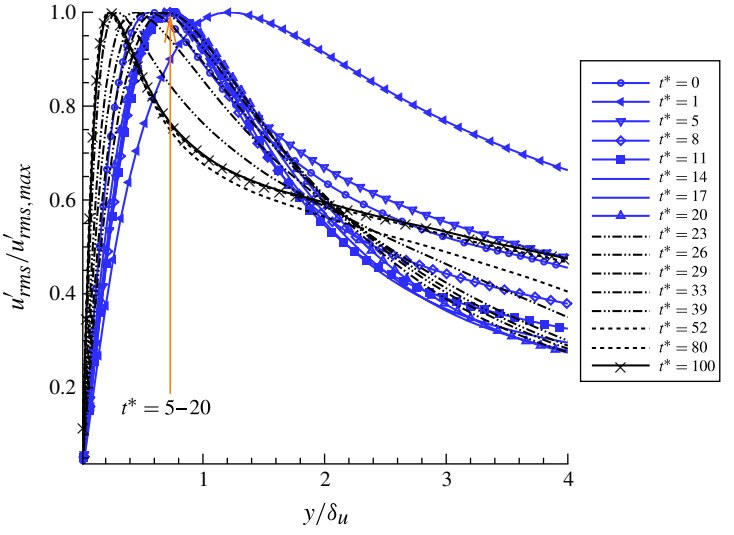


FIGURE 13. (Colour online) Development of streamwise r.m.s. velocity profile normalized by its peak value. The horizontal axis is normalized by the displacement thickness based on the full velocity field.

data show that they remain largely unchanged during this period. Both $(v'_{rms}/U_{b1})^2_{max}$ and $(w'_{rms}/U_{b1})^2_{max}$ increase rapidly over the transitional period while $(u'_{rms}/U_{b1})^2_{max}$ continues to increase linearly initially but becomes saturated about halfway into the transitional period and reduces afterwards. Contrasting the observations in boundary layer transition by for example Matsubara & Alfredsson (2001), where the onset of transition causes an exponential increase in energy growth rate, in the present flow, the rate of growth of $(2k/U^2_{b1})_{max}$ only increases gently following the transition. Its reduction in the second part of the transition is consistent with observations in boundary layer bypass transition.

Figure 13 shows the evolution of the non-dimensional profiles of $(u'_{rms}/U_{b1})_{max}$ versus y/δ_u, where δ_u is the velocity displacement thickness based on the full flow

https://doi.org/10.1017/jfm.2012.498 Published online by Cambridge University Press

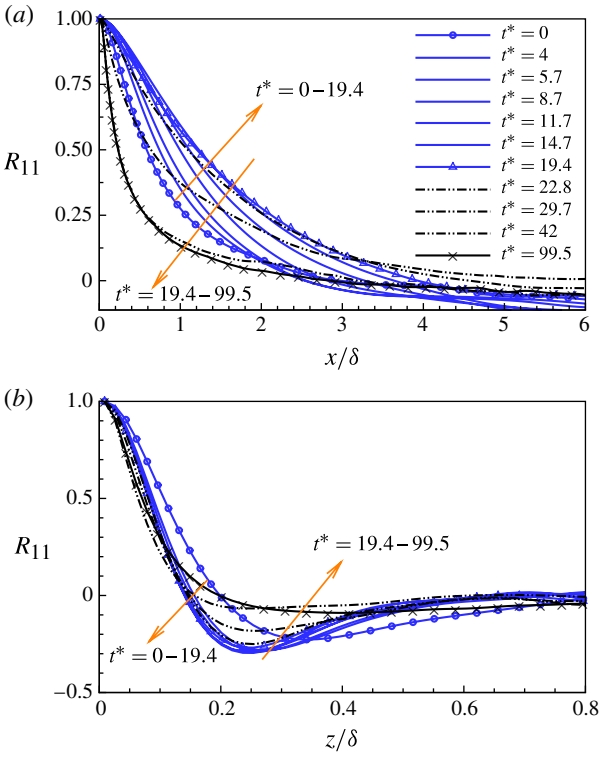


FIGURE 14. (Colour online) Development with time of profiles of (*a*) streamwise and (*b*) spanwise correlations of the streamwise velocity at $y/\delta_u = 0.8$.

field velocity $\overline{u}$ (not $\overline{u}\hat{}$). During most of the pre-transitional stage, the profiles at different times exhibit strong similarity with the peak location centred at $y/\delta_u \sim 0.75$. This suggests that the u' profile grows with the growth of the time-developing boundary layer and is scaled with the boundary layer thickness rather than the inner scaling, hence deviating from typical turbulent flows. This is again a feature of bypass transition that has been discussed by various researchers, but is different from them in that the peak location is at $\sim 0.75\delta_u$ rather than the typical value of $1.3\delta_u$. This is likely to be the effect of the initial velocity profile that plays an important role in the transient flow transition, contrasting with the uniform velocity profile outside an external boundary layer. In fact, with respect to δ_{du} based on the differential velocity ($\overline{u}\hat{}$), the location is in the range of $1.1\delta_{du}$–$1.4\delta_{du}$, which is closer to that of the boundary layer transition but it does not remain constant anymore. The results in figure 13 also show that, during the transitional period, the location shifts towards the wall and eventually settling at $y/\delta_u \sim 0.2$, or $y^+ = 15$, as expected for a fully developed turbulent flow.

3.2.3. *Correlations and spectra*

The correlation of the streamwise velocity (R_{11}) can be used to provide quantitative information on the streaks. The streamwise correlation provides a measure of the length of the streaks whereas the spanwise correlation measures the spacing between the streaks. It can be seen from figure 14(*a*) that the streamwise correlation increases progressively during pre-transition indicating that the averaged length of the streaks

https://doi.org/10.1017/jfm.2012.498 Published online by Cambridge University Press

increases during this period. Soon after the onset of the transition, the correlation and hence the streak length reduces, reaching the steady flow profile at the end of transition ($t^* = 42$).

In boundary layer bypass transition, it has been shown that the spanwise correlation exhibits a negative value during pre-transitional and transitional periods owing to the presence of streaks (e.g. Jacobs & Durbin 2001; Matsubara & Alfredsson 2001). Twice the distance at which minimum R_{11} occurs (z_{min}) is used to define the spacing of the streaks which is generally double the thickness of the boundary layer. Such correlations at $y/\delta_u = 0.8$ are shown in figure 14(*b*) for several time instants throughout the flow transient. There is clearly a minimum in the correlation during the pre-transitional and the early transitional periods. The value is about -0.30 just before the onset of the transition, which is smaller than the typical value of -0.35 found in the boundary layer bypass transition (Matsubara & Alfredsson 2001). The distance at which the minimum R_{11} occurs (z_{min}/δ) varies non-monotonically, starting from the highest value ($\sim$0.3), first decreasing rapidly to the minimum (0.23) but then increasing slowly. The spacing of the streaks ($2z_{min}$) at the time of the onset of transition is about twice the boundary layer thickness which is again consistent with boundary layer transition. It is interesting however that there is a minimum negative correlation in the initial steady flow indicating that streaks are present then. For boundary flow flows, this is clearly not the case and the streaky structures only form after some distance from the leading edge, as for example shown in figure 10 of Matsubara & Alfredsson (2001).

The detailed flow structure can be illustrated more effectively using a contour plot of spanwise correlation at various distances from the wall, following Matsubara & Alfredsson (2001). Figure 15 shows such plots at several time instants throughout the transient, together with a reproduction of figure 12 from the above reference. The corresponding boundary layer thickness in Matsubara & Alfredsson (2001) is 11 mm and the data show that the negative correlations are confined within the boundary layer and z_{min} is about the size of the boundary layer. Our data on transient channel flow show a more complex picture that evolves with time. There is clearly a minimum point present in the initial steady flow at about $y/\delta = 0.06$ (or $y^{+0} \sim 15$) with $(z/\delta)_{min} = 0.3$, and further troughs in the core of the flow located at larger z/δ. This reflects the fact that there are turbulent structures of various length scales in the initial flow. The spacing/size of the structures near the wall are smaller than those in the core. In comparison, the FST at the leading edge of the boundary layer would have no such structures and the contour plot would comprise only vertical lines. It is clear from the contour plots in figure 15 that during the pre-transitional period, the initial near-wall structures are modulated and enhanced. The near wall structures are enlarged in figure 15(*b*) for more detailed inspection. During the early stage ($t^* < 12$), the spacing and the vertical location of these initial streaky structures are adjusted, accompanied by an increase in intensity. The value of $(z/\delta)_{min}$ is reduced from 0.3 to 0.23 as already identified above and the vertical location is lowered down somewhat towards the wall initially (see $t^* = 4$) but regains the height at $t^* = 12$. Such modulation of the initial streaky structures by the new boundary layer can be compared with the receptivity stage of boundary layer bypass transition during which streaks, which are initially non-existent, develop in response to leading-edge/FST disturbances. Referring to figure 13, this period ($t^* < 12$) appears to coincide with the stage when a similarity of the profiles of $(v'_{rms}/U_{b1})^2_{max}$ is being formed. During the remaining period of pre-transition, the near-wall structures in figure 15 appear to further grow outwards slightly before the onset of transition.

https://doi.org/10.1017/jfm.2012.498 Published online by Cambridge University Press

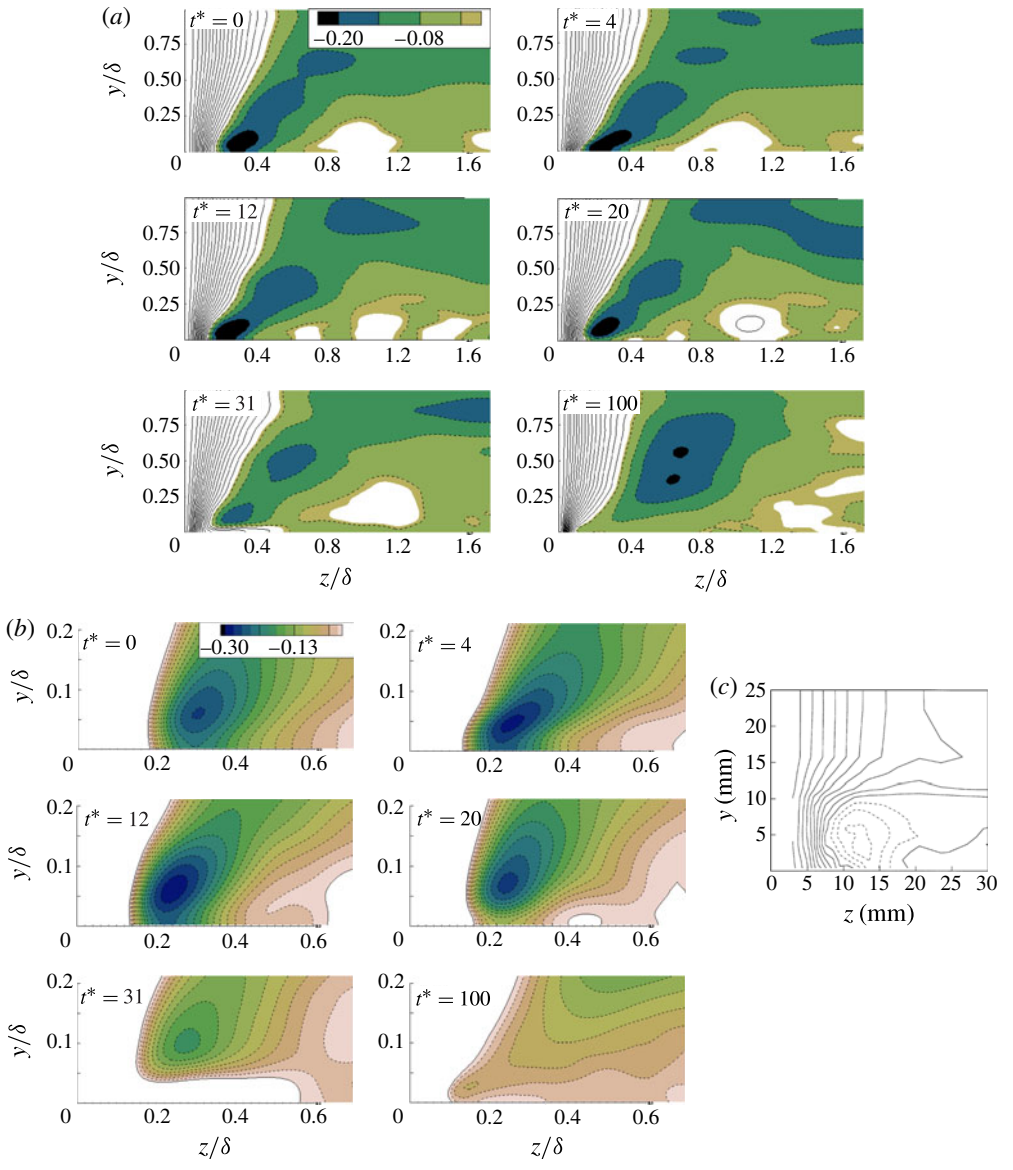


FIGURE 15. (Colour online) Time sequences of contours of the spanwise correlation of the streamwise velocity at various heights above the wall. Solid lines are positive and broken lines are negative values. Also, negative values are shaded; positive values are in white. (*a*) Full flow field; (*b*) near-wall structures (only negative value contours are shown); (*c*) boundary layer bypass transition reproduced from Matsubara & Alfredsson (2001).

Figure 16 shows the pre-multiplied streamwise and spanwise wavenumber spectra ($k_z^0 E_{11}^0/U_{\tau_0}^2$) of the streamwise velocity at $y/\delta_u = 0.8$. The main figures are presented in log–linear scales but the inset at the top is in log–log scale to facilitate the study of the early responses in the high-wavenumber region. Following the commencement of the flow transient, the energy spectrum of high wavenumbers ($k_x^{+0} > 0.025$) of the streamwise $k_z^0 E_{11}^0/U_{\tau_0}^2$ reduces rapidly reaching a minimum around $t^* \sim 4$, before

https://doi.org/10.1017/jfm.2012.498 Published online by Cambridge University Press

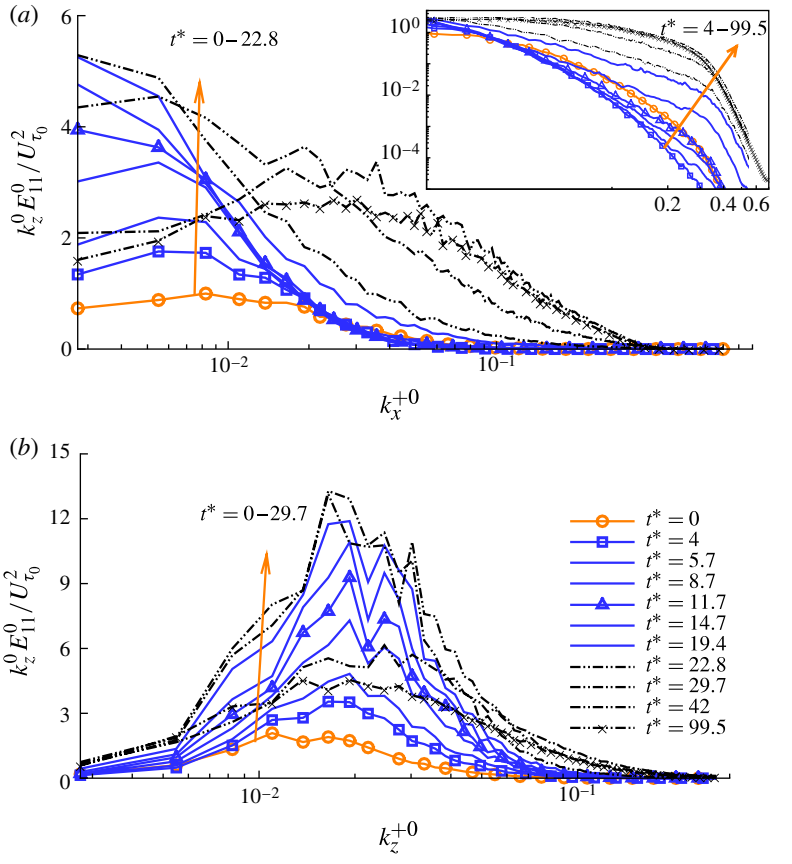


FIGURE 16. (Colour online) Development of pre-multiplied (*a*) streamwise and (*b*) spanwise wavenumber spectra at $y/\delta_u = 0.8$ normalized using initial steady flow parameters. Inset shows a log–log plot of a part of the spectra.

increasing again first from the high-wavenumber region, and gradually moving towards the lower-wavenumber region. In the low-wavenumber region ($k_x^{+0} < 0.025$), the energy increases immediately following the start of the transient which continues until $t^* \sim 20$, and then remains largely unchanged until towards the end of the transition, when it drops to a typical shape for a turbulent flow. These changes in the low-wavenumber spectrum imply that, following the start of the transient, the energy of the large structures immediately increases, which continues during the early stages of the pre-transitional phase as a result of the elongation of the streaks, but reaches saturation before the onset of the transition. The reduction of the energy towards the end of the transition can be interpreted as the breaking up of the elongated streaks.

Small turbulent structures (or high wavenumbers) on the other hand are damped at the beginning of the flow transient which seems to be consistent with the well-established observation of a sheltering effect in boundary layer transition, namely, it is difficult for high-frequency FST to penetrate into the boundary layer (see for example Jacobs & Durbin 2001). However, the energy of small structures starts increasing rather early during the pre-transitional period, first in the high-wavenumber region, then moving into the lower-wavenumber region. It is of interest to note the rather

https://doi.org/10.1017/jfm.2012.498 Published online by Cambridge University Press

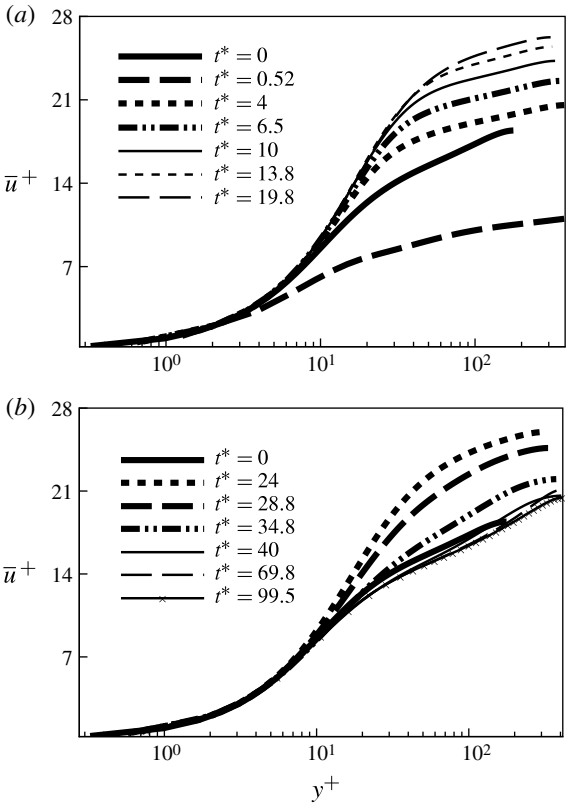


FIGURE 17. Profiles of mean velocity at different time instants in a transient flow: (*a*) pre-transitional phase; (*b*) transitional and fully turbulent flow phases.

'independent' responses of the high- and low-wavenumber turbulence structures, which appears to suggest that the energy generation of turbulence in the pre-transitional and transitional periods does not follow the typical energy cascades. Considering the spectrum at $t^* = 11.7$ (inset in figure 16*a*), for example, the high-wavenumber energy is increased in comparison with that at early times, which is probably associated with the generation of small turbulent spots, being very sparse and isolated at this stage. This occurs without any changes in the energy in the medium wavenumbers. At later times, as the turbulent spots grow in size and join with each other, the medium and lower spectrum energy grows. This continues until the full surface of the wall is covered with new turbulence ($t^* = 42$) when the spectrum assumes the typical distribution of fully developed turbulence.

The spanwise spectra of the streamwise velocity show a rather different picture. The energy shows an overall trend of increase across the entire spectrum during the pre-transitional and the transitional periods. This is consistent with the observations of Matsubara & Alfredsson (2001).

3.2.4. *Mean and r.m.s. velocities*

Figure 17 shows the ensemble-averaged mean velocity profiles in a semi-logarithmic form, with results in the pre-transitional phase shown in (*a*) and those in the transitional and fully turbulent phases shown in (*b*). During the pre-transitional period,

https://doi.org/10.1017/jfm.2012.498 Published online by Cambridge University Press

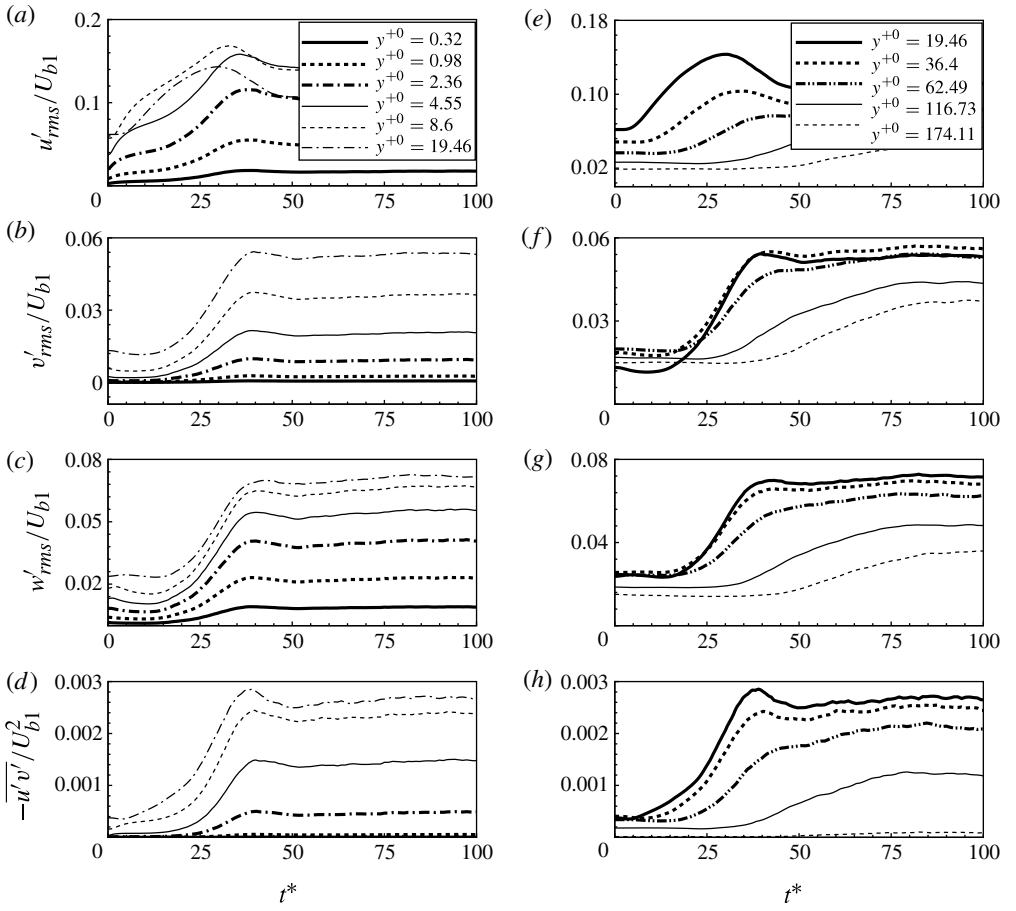


FIGURE 18. Development of the normalized r.m.s. of the fluctuating velocities and turbulent shear stress: (*a–d*) near wall; (*e–h*) core region.

after a rapid reduction at the very early stage, the logarithmic velocity profile gradually increases with time reaching a maximum around the time of the onset of the transition. At this stage, the sub-layer becomes much thicker. After the transition begins, the velocity in the core progressively reduces and reaches the steady flow profile at around $t^* = 42$, i.e. at the end of the transition. This trend is similar to that of a boundary layer transition, see for example Nolan *et al.* (2010).

Figure 18 shows the time development of the ensemble-averaged r.m.s. of the fluctuating velocities normalized by the final bulk velocity (u'_{rms}/U_{b1}, v'_{rms}/U_{b1} and w'_{rms}/U_{b1}) and that of the normalized turbulent shear stress ($-\overline{u'v'}/U_{b1}^2$). The key features of these statistics in our transient channel flow agree well with available experimental results of pipe flows. Maruyama *et al.* (1976) showed that the response of u' is strongly dependent on the radial location, from which they derived that in transient flows, turbulence is first generated in the wall region and then propagates into the core with time. With measurements of all three normal turbulent stresses and the shear stress obtained from an LDA system, He & Jackson (2000) established that u'_{rms} responds first near the wall, followed by v'_{rms} and w'_{rms} together, and that the spatial diffusion plays an important role in the response of turbulence in the core of the flow.

https://doi.org/10.1017/jfm.2012.498 Published online by Cambridge University Press

Our data consolidate these previous observations and add more detailed information, especially in the wall region where the most interesting turbulent activities occur but measurements are lacking due to technical difficulties. However, our main interest here is to relate the variations of flow statistics to the transition phenomena discussed above.

We first consider the response in the pre-transitional period ($t^* < 20$) and limit ourselves to the near-wall region as there is little activity beyond this region during this period. The response of the axial velocity (u'_{rms}) and that of the other two components (v'_{rms} and w'_{rms}) shown in figure 18 are categorically different. The value of u'_{rms} increases progressively, immediately after the commencement of the transient at locations adjacent to the wall, but with a small delay at locations away from the wall ($y^{+0} > 5$), whereas v'_{rms} and w'_{rms} remain unchanged or at some locations reduce slightly during the same period. It is now clear that these responses are reflections of the pre-transitional flow behaviour. The increase of u'_{rms} is a reflection of the stretching of the eddies pre-existing in the flow field before the start of the transient, resulting in the streaks of axial fluctuating velocities observed earlier in § 3.1. These results show that, statistically, the stretching of the eddies initially starts from the wall, progressing into the core and reaching the location $y^{+0} < 50$ just before the onset of transition. The maximum u'_{rms}/U_{b1} at the start of transition ($t^* = 20$) is $\sim$14 % which is higher than the theoretical critical streak amplitude of $\sim$10 % predicted by Vaughan & Zaki (2011) and the maximum r.m.s. streak amplitude of $\sim$9 % in the experiments of Mandal *et al.* (2010) for external boundary layer bypass transition. Notwithstanding the significant increases in u'_{rms} (and hence the overall turbulent kinetic energy) in the pre-transitional period, the wall friction only deviates slightly from the Blasius solution for a laminar flow as seen in figure 9. The results also show that the stretching of eddies has little effect on v'_{rms} and w'_{rms} anywhere in the flow including the wall region. In effect, the flow is laminar-like, or pseudo-turbulent, before the onset of transition, resembling the buffeted laminar flow in the boundary layer bypass transition.

During the transitional period, u'_{rms} continues increasing (but at a faster speed close to the wall, $y^{+0} < 10$) until about halfway (i.e. about $t^* = 35$), when it reaches a maximum, overshooting the steady values, after which it reduces and eventually approaches the steady values towards the end of the transition. Both v'_{rms} and w'_{rms} again show a similar trend to each other but different to that of u'_{rms}, both increasing monotonically to a peak value close to the end of the transition. It is apparent that these increases are associated with the generation and growth of turbulent spots which have the effect of transferring energy from u'_{rms} to the other two components, implying that a direct result of the generation of turbulent spots is a reduction of the energy of the axial turbulent fluctuations. Another effect on u' is that the large structures of streaks containing the energy of u' before the generation of turbulent spots are broken down into smaller structures causing changes in the spectra of u'. The continual increase of u' in the early stages of the transitional phase is partly due to the fact that most of the wall surfaces are still covered by streaks which are being stretched extracting more energy from the mean flow. During the later stages, there is a net consumption of the energy of u' as turbulent spots spread, redistributing more energy from u' to the other two components, and hence a reduction in u'.

From the instantaneous flow pictures presented earlier, it is not difficult to deduce that the gradual increase of the ensemble-averaged r.m.s. velocities in the transitional phase is not a true reflection of the fluctuating velocities at any particular location. To a great degree, the velocity at any location is either quasi-laminar (before transition reaching that particular location) or turbulent (after the transition). When the flow at

https://doi.org/10.1017/jfm.2012.498 Published online by Cambridge University Press

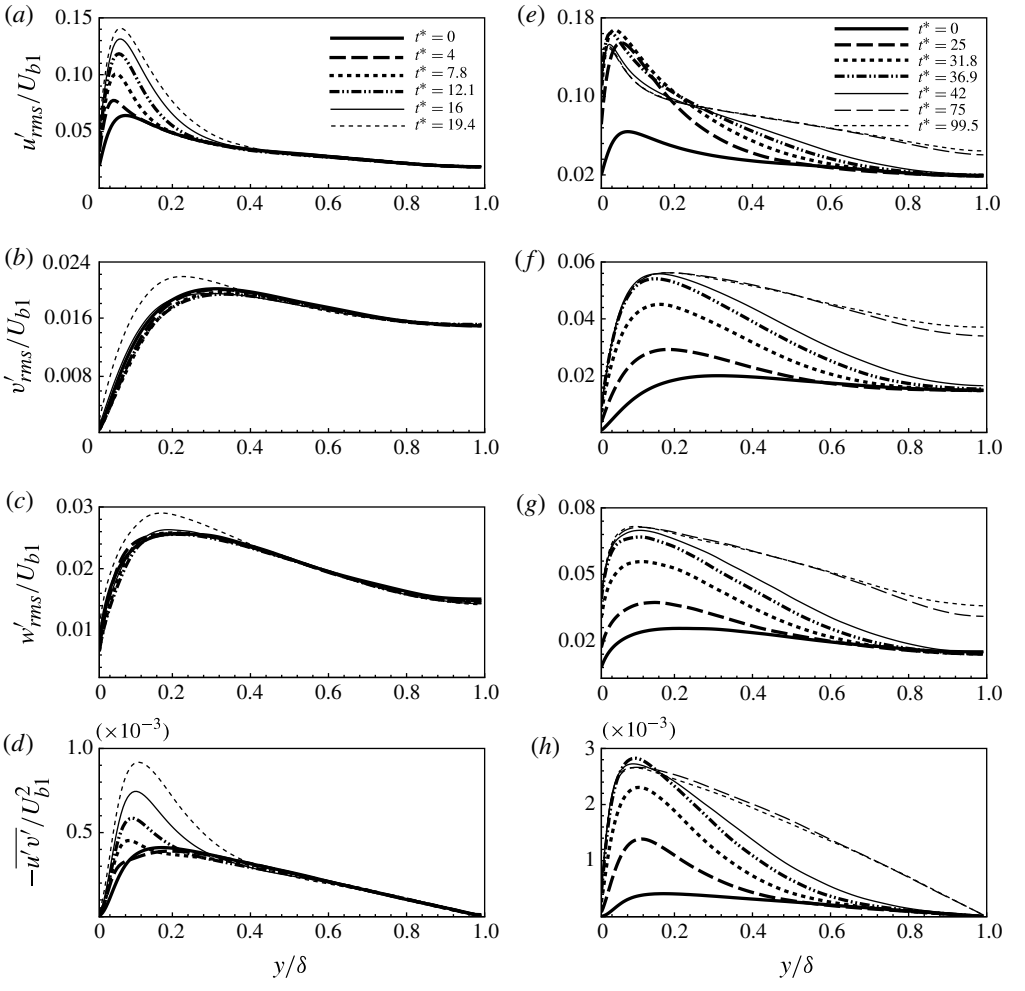


FIGURE 19. Profiles of the normalized r.m.s. fluctuating velocities and turbulent shear at several instants during a transient flow; (*a–d*) pre-transitional phase and (*e–h*) transitional and fully turbulent phases.

any location is turbulent, the intensity remains more or less unchanged (figure 4). The increasing r.m.s. values during the transitional phase result from the gradually increasing surface area of the wall occupied by turbulence. The turbulent shear stress is also shown in figure 18 for completeness. In the core of the flow its response is similar to that of the normal stresses, remaining little changed until nearly the end of the transition before increasing and approaching the steady value well after the completion of the transition. In the wall region, say $y^{+0} < 50$, the development of $-\overline{u'v'}$ can be divided into several stages: (i) it increases slowly during the pre-transitional phase; and (ii) at a much faster rate after the transition starts, reaching a maximum at about halfway into the transition; after which (iii) it reduces and approaches the steady values during the second part of the transition; and (iv) fluctuates around these values afterwards.

Figure 19 shows the profiles of the ensemble-averaged r.m.s. of the fluctuating velocity and turbulent shear stress at various times. It can be seen that, before the

https://doi.org/10.1017/jfm.2012.498 Published online by Cambridge University Press

transition ($t^* < 20$), the response of u'_{rms} is limited to $y^{+0} < 50$ (i.e. $y/\delta \sim 0.3$) and that the response first occurs close to the wall, and then expands into the core of the flow as time progresses. During the transition, ($20 < t^* < 42$), the region of the response of u'_{rms} continues to grow. For a notable period, u'_{rms} in the wall region significantly overshoots the steady values. At the end of the transition ($t^* = 42$), the u'_{rms} value at the centre of the channel has hardly changed from its initial value. It only reaches the steady profile at a much later time of $t^* = 75$. Again, v'_{rms} and w'_{rms} behave differently from u'_{rms}. At the early stages of the pre-transitional period, both quantities show an overall trend of reduction albeit only slight. Then, when v'_{rms} and w'_{rms} do respond, they do so simultaneously in a rather broad region. The behaviour of the turbulent shear stress $-\overline{u'v'}$ is in between that of u'_{rms} and v'_{rms} and w'_{rms}. The value of $-\overline{u'v'}$ is doubled in the pre-transitional period but this change is actually rather small in comparison with the corresponding steady value. It is also clear that at the end of the transition, the profile is still far from the linear distribution in the core of the flow (characteristic of a fully developed flow). In fact, on completion of transition, the full span of the surface of the wall is filled with turbulence, but much of the core of the flow is still disconnected from the new turbulence. The flow continually adjusts for a further period of time ($t^* = 42$–75) as the turbulence gradually propagates into the core. This is reflected in the friction coefficient but only as a very small increase. The fully turbulent phase can therefore be subdivided into a post-transition ($t^* = 42$–75) and a fully developed turbulent stage (beyond $t^* = 75$), although there are only very subtle differences in turbulence near the wall during these two stages.

3.2.5. *The budget of the r.m.s. velocities*

The purpose of this section is to discuss the connections between the instantaneous flow structures and the budget terms of the fluctuating velocities. To this end, the time variations of the production, dissipation and pressure–strain terms for u'_{rms}, integrated over the half-height of the channel, are shown in figure 20 to illustrate the development of the main budget terms over time. It can be seen that the production increases linearly with time during the pre-transitional phase, but only reaching ~20 % of the final value at the end of this period ($t^* = 20$). It increases at a much greater rate during the transitional phase reaching approximately the steady value towards the end of this period ($t^* = 42$), followed by a relaxation period ($42 < t^* < 75$) before settling to the steady value. The dissipation follows a similar trend whilst the pressure–strain term remains effectively unchanged during the pre-transitional period, increasing rapidly to the steady value during transition. It is interesting to compare these with the variation of the r.m.s. velocities. As can be seen from figure 12, $(u'_{rms})_{max}$ increases linearly during the pre-transitional period, approaching the steady values at the end of this period ($t^* = 20$), contrasting strongly with the production and dissipation which are only a fraction of their respective steady values. This shows an interesting scenario whereby energy is extracted from the mean flow to significantly increase the turbulent kinetic energy, with only a small increase in the energy dissipation rate. In fact, as has been established in this paper, there is hardly any production of 'true' turbulence during the pre-transitional period and the turbulent kinetic energy calculated from the statistics of the flow is a measure of the fluctuating velocity due to the elongated streaks, which are large coherent structures resulting from the stretching of the turbulent eddies present in the initial flow.

In the boundary layer transition, a similar flow (the buffeted laminar flow) is formed as a result of receptivity to the FST. As can be seen from figure 9, the friction coefficient at this stage is close to the Blasius laminar flow solution,

https://doi.org/10.1017/jfm.2012.498 Published online by Cambridge University Press

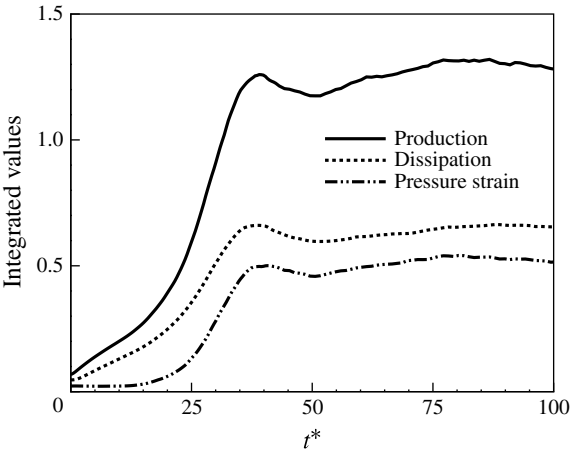


FIGURE 20. Development of the budget terms of u' integrated over the half -channel height normalized with $U_{\tau_0}^4/\nu\delta$.

deviating significantly from the typical turbulent values. During the transition, the production increases exponentially with time but the overall turbulent kinetic energy only increases in the first half of the transition period, reducing afterwards. In fact, during this period, some energy stored in the elongated streaks is turned into energy of much smaller structures as turbulent spots are generated, resulting in energy transfer from u' to v' and w' without increasing the total energy. More importantly, new turbulence structures generated dissipate energy at a much faster rate, as expected in a typical turbulent flow. Another point to note is the important implication of the development of the pressure–strain term, which is a sink for u' but the main energy source for v' and w'. During the pre-transitional period, the pressure–strain term remains largely unchanged, which results in the non-varying development of v' and w' in this period, demonstrating that no 'conventional' turbulence is produced during the pre-transitional period. In this context, the pressure–strain term is a useful parameter which can be used to indicate the onset of transition and to 'measure' the percentage of the completion of transition.

Figure 21 shows the spatial distribution of all budget terms of u' normalized with U_τ^4/ν at several time instants together with the budget terms for the corresponding final steady flow. This illustrates the deviation of the distribution of the budget from that of an equilibrium steady flow during various stages of the transition. Unlike the results in figure 20, these data, normalized with the ensemble-averaged friction velocity at the corresponding time, do not show the absolute variations during the transitional period. Immediately following the commencement of the transient, the normalized budget terms reduce to very low values due to the rapid increase of wall shear stress. All terms except the pressure–strain term increase significantly over the pre-transitional period ($t^* < 20$), approaching the steady values by the end of this period. However, the distributions are characteristically different from those of a typical turbulent wall shear flow. First, the location of the peak production is at $y^+ = 20$ which is significantly different from the typical value of $y^+ = 10$. Secondly, the dissipation remains rather uniform in the wall region (say, $y^+ < 20$), whereas a typical feature of wall shear flow is that the dissipation increases as the wall is approached. Thirdly, as noted before, the pressure–strain term remains very low, which implies that no energy is supplied

https://doi.org/10.1017/jfm.2012.498 Published online by Cambridge University Press

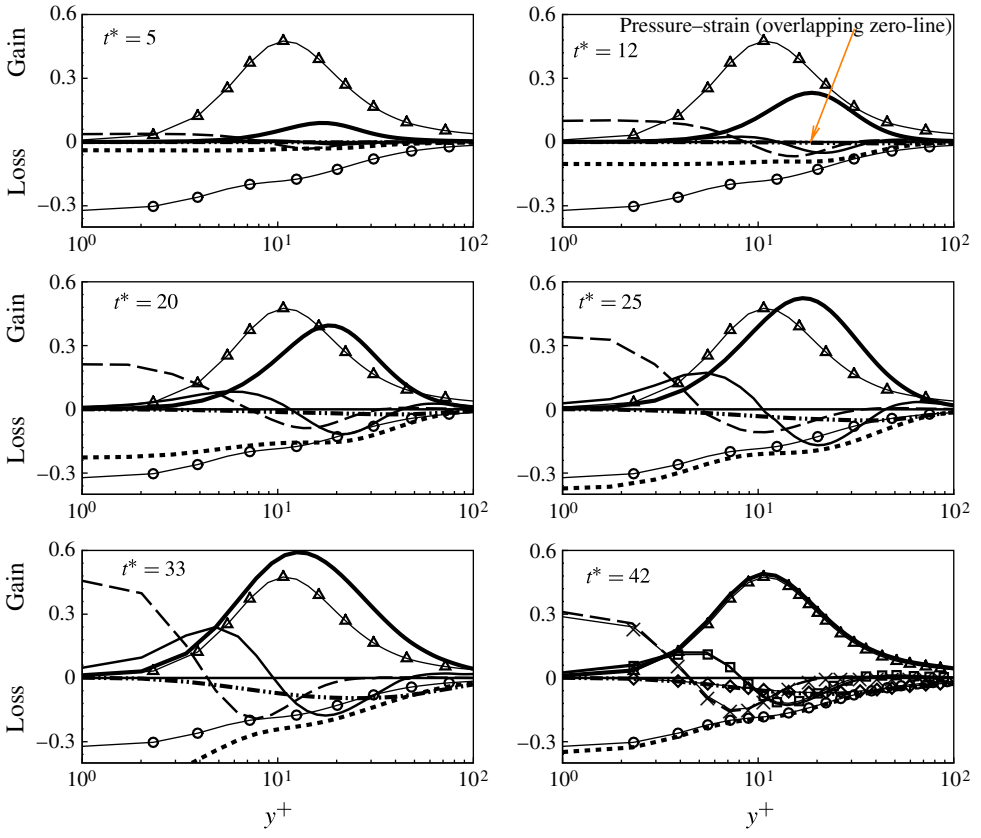


FIGURE 21. (Colour online) Distribution of the budget terms of u' normalized with U_τ^4/ν at several time instants during the transient (lines) compared with those of the final steady flow (markers). Some of the terms of the steady flow are removed to improve the readability. (Transient: thick solid line, production; short-dashed line, dissipation; dash dot dot line, pressure strain; long-dashed line, viscous diffusion; thin solid line, turbulent transport. Final steady flow: triangle, production; circle, dissipation; diamond, pressure strain; cross, viscous diffusion; square, turbulent transport.)

to v' and w'. Clearly these are features of the budget of the statistics of the elongated streaky structures before the transition ($t^* = 20$) rather than those of a typical turbulent flow. Later during the transition, the differences between the unsteady and steady distributions reduce and eventually disappear, and at $t^* = 42$, the budget distribution overlaps that of a steady flow.

4. Summary and conclusions

The behaviour of turbulence in a transient channel flow following a rapid increase of flow rate from an initially turbulent flow at a low Reynolds number has been investigated using DNS. Flow visualizations along with detailed analysis of flow statistics, including correlations and spectral analysis of fluctuating velocities, budget of turbulent stresses and the evolution of the mean velocity and turbulent stresses, are used to study the detailed characteristics of the flow. It is shown that the development of the transient turbulent flow is not a progressive evolution from the initial turbulent

https://doi.org/10.1017/jfm.2012.498 Published online by Cambridge University Press

flow to a new one. Instead, the flow undergoes a transition that is strikingly similar to a boundary layer bypass transition subject to FST. The key findings are summarized below.

4.1. *General description of the transient channel flow transition*

Following a rapid increase of flow rate, a thin boundary layer of high strain rate is initially formed adjacent to the wall, which grows outwards into the flow with time. This time-developing boundary layer is the main source of further change of flow structures. The turbulence pre-existing in the flow before the commencement of the flow transient provides disturbances to this new boundary layer much like the role that the FST plays in the external boundary layer bypass transition. The development of the flow undergoes three phases, namely, pre-transition, transition and fully turbulent flow, resembling the three regions of the boundary layer bypass transition, namely, the buffeted laminar flow, the intermittent flow and the fully turbulent flow regions.

In the pre-transitional phase, the initial near-wall turbulence structures are selectively modulated forming elongated streaks of streamwise velocity with low spanwise wavenumbers. The streaks formed are further enhanced with time but overall the flow structures are stable and the changes are progressive at this stage.

In the transitional phase, the flow becomes unstable and turbulent spots are being generated. We have observed that in most cases the generation of turbulent spots appears to be associated with a backward jet detached from the wall, with a forward jet formed underneath it. Disturbances from outside the boundary layer appear to interact with such backward jets, destabilize them and eventually lead to the formation of three-dimensional turbulent spots, which is accompanied by the generation of hairpin vortical structures. The turbulent spots generated grow in both the streamwise and the spanwise directions and eventually merge with each other. This spreading takes a substantial period of time. When the turbulent regions have spread to cover the full span of the wall surfaces, the transition is complete and the flow is said to enter a fully turbulent phase.

The fully turbulent phase can be subdivided into a post-transitional stage and a fully developed turbulent flow stage. At the end of the transitional phase, all wall surfaces are covered with newly generated turbulence but its existence is still limited to the wall region, whereas the core of the flow remains little affected. It takes a significant period of time for the newly formed turbulence to propagate into the core. During this post-transitional period, turbulence quantities in the core increase significantly to reach the corresponding steady values, but this has only a minimal effect on the turbulence in the wall region and the friction coefficient. The flow becomes fully developed and the statistics exhibit features of universal distributions once this process has completed.

The process of the transition appears to occur independently in the top and bottom wall layers as if two boundary layer bypass transitions were occurring simultaneously but did not ‘talk’ to each other. This process is different from the typical subcritical plane channel transition in low-Reynolds-number flows where turbulent spots occupy the full channel height from early stages before spreading spanwise over the plane.

The time-developing boundary layer is quantitatively described by using the change of the flow from its initial profile, namely, $\overline{u}(y/\delta, t^*) - \overline{u}(y/\delta, 0)$, which has been directly compared with the external boundary layer transition by relating the time of the transient flow with the downstream distance of the boundary layer through a convection velocity. It has been shown that the velocity profile and friction coefficient in the pre-transitional phase follow closely the Blasius laminar boundary layer solution. In addition, the friction coefficient during the entire transition process is consistent

https://doi.org/10.1017/jfm.2012.498 Published online by Cambridge University Press

with the experimental results of Roach & Brierley (1992) of a boundary layer transition scenario. The development of the momentum-thickness Reynolds number and the shape factor in the transient channel flow also closely resemble that of the boundary layer.

It is however of interest to note the differences between the flow conditions/disturbances in the transient flow that we are concerned with herein and those in a typical external boundary layer.

(i) Typically the FST in a boundary layer transition is isotropic, homogeneous when generated at the inlet and decays with distance. There is little interaction between FST and the uniform mean free-stream flow.

(ii) The 'FST' in the transient flow considered herein is a typical low-Reynolds-number shear flow: anisotropic, inhomogeneous, containing streaky structures, and the mean flow and turbulence outside the boundary layer continue interacting with each other and the overall turbulence level remains largely unchanged during the transition.

4.2. *Characteristics of streaks*

The correlation of the streamwise fluctuating velocity and the wavenumber spectra provide quantitative information on the development of the flow structures. The streamwise correlation shows that the integral length scale increases progressively during the pre-transitional period, reaching a maximum around the time of the onset of transition, reflecting the formation and elongation of streaks. Following the start of the transition, the length scale reduces gradually as the streaks are broken up and smaller turbulent structures are generated, eventually assuming a typical profile of a turbulent flow at the end of the transitional period, which remains unchanged over the post-transitional relaxation period. The contour plots of the spanwise correlation in the y–z plane clearly show the presence of streaky turbulent structures in the initial steady flow which are expected in low-Reynolds-number turbulent flows. During the early stage of the pre-transition ($t^* < 12$), the near-wall streaks are modulated into structures with significantly reduced spacing ($(z/\delta)_{min}$ reducing from 0.3 to 0.23) and an increased strength, forming the elongated streaks that are typically seen in the buffeted laminar flow region of a bypass transition. During the late stage of the pre-transitional period ($12 < t^* < 20$), the spacing of these structures grows slowly in line with the increase of the boundary layer thickness but the strength (minimum spanwise R_{11}) remains largely unchanged. In view of the formation of elongated streaks, the early stage of the pre-transition is equivalent to the receptivity of bypass transition, but the fact that these are building upon pre-existing streaky structures in the initial turbulent flow makes them contrast strongly with external boundary layers studied previously.

The wavenumber energy spectra show further characteristics of the flow structures of the transient flow. The structures of high wavenumbers ($k_x^{+0} > 0.025$) and low wavenumbers ($k_x^{+0} < 0.025$) are clearly disconnected and evolve independently of each other, and the turbulence energy cascade law does not appear to describe the flow structures of the transition completely. The elongation of streaks during the pre-transitional period is reflected as an increase in the energy of the low-wavenumber structures which continues until about $t^* = 20$. In contrast, the energy of the high-wavenumber structures is significantly reduced at the early stage of the pre-transitional period, being consistent with observations in the bypass transition, which shows that high-frequency disturbances are suppressed by the boundary layer. Interestingly in the high-wavenumber domain, when new energy is re-generated, it is first exhibited

https://doi.org/10.1017/jfm.2012.498 Published online by Cambridge University Press

as very high-wavenumber structures and appears long before the onset of transition. The energy growth then spreads towards lower wavenumber regions during the late pre-transitional and transitional periods. This process is likely to be linked to the initial generation of isolated turbulent spots and the subsequent growth and spread of turbulent regions.

4.3. *Energy growth*

Linear energy growth of disturbances, an important characteristic of boundary layer bypass transition, is observed in the transient channel flow considered herein. The energy of the streamwise fluctuations and the turbulent kinetic energy increases linearly in the pre-transitional period, and the distribution of u'_{rms} develops into a self-similar profile which grows with the boundary layer thickness. Additionally, it is seen that the energy of v' and w' remains essentially unchanged in the same period. Unlike observations in some boundary layer transition investigations, there is no exponential increase in the energy growth rate following the onset of transition. In addition, the location of the peak u'_{rms} is significantly closer to the wall in the present flow in relation to the velocity displacement thickness ($0.75\delta_u$ as opposed to $1.3\delta_u$). This is likely to be due to the fact that the 'free-stream flow' beyond the newly developed boundary layer is part of a velocity profile of a turbulent channel flow rather than a uniform flow.

The analysis of the budget terms of u'_{rms} is used to explain the mechanisms of the energy growth. Both production and dissipation grow linearly in the pre-transitional period but at a rate significantly lower than the rate of growth of the energy itself. It is clear that the elongated streaks contain high energy which dissipates at a significantly lower rate than that in a turbulent flow with the same level of velocity fluctuations. The spatial distribution of the budget terms deviates significantly from that of a typical wall shear flow, in particular with the peak production located further away from the wall. Also significantly different from a turbulent flow is the dissipation, which increases sharply approaching the wall in a turbulent shear flow, but is rather flat in the wall region in the transient flow during the pre-transitional period. The pressure–strain term is a key parameter which is capable of reflecting the true characteristics of the flow. It remains unchanged before the onset of the transition and increases rapidly during the transition along with an increase in the turbulent spots, and is hence a useful parameter for unambiguously determining the onset of transition.

4.4. *Evolution of the mean and turbulent velocities*

The development of the mean velocity and turbulent stresses in the transient channel flow obtained from the DNS agrees well with previous experimental results of flows in a pipe with a stepwise increase of flow rate and those with a linear flow acceleration. In addition, the present study provides detailed data for the near-wall region which are not available from previous experimental studies. However the main contribution of the present study on flow statistics is to reinterpret the unsteady flow data in a coherent way using the new understanding developed. Both the present study and previous investigations show that u' increases immediately following the start of a flow transient, often over-shooting the quasi-steady values in the early stages, whereas v' and w' remain unchanged for a rather long period before increasing rapidly. It is now understood that the initial increase of u' is due to the formation of elongated streaks which are not 'conventional' turbulence but large coherent structures. The flow at this stage is laminar-like or pseudo-turbulent, resembling the buffeted laminar flow in the

https://doi.org/10.1017/jfm.2012.498 Published online by Cambridge University Press

boundary layer bypass transition. This explains the reason why the friction coefficient agrees well with the Blasius laminar flow solution even when turbulent kinetic energy over-shoots the steady values. During this period, the energy extracted from the mean flow is much less than in a typical turbulent flow despite the high 'turbulence' level. The response of v' and w' marks the onset of transition and the generation of new turbulence.

The gradual increase of the ensemble-averaged r.m.s. velocities measured during the responding phase (i.e. transitional period) is not a true reflection of the fluctuating velocities at any particular location. In reality, the flow at any particular location is either quasi-laminar (before transition occurs at that particular location) or turbulent after the transition. The increase of the ensemble-averaged r.m.s. values results from the gradually increasing regions of the flow occupied by turbulence.

Acknowledgements

The work is funded by UK Engineering and Physical Science Research Council (EP/G068925/1). We gratefully acknowledge fruitful discussions with Professor A. Vardy and Dr C. Ariyaratne over many years and advice from Professor P. Orlandi in numerical methods. We are also grateful to the anonymous reviewers for their very useful suggestions which have helped to significantly improve the paper.

Appendix. Numerical methods

Equations (2.1) and (2.2) are discretized on a rectangular staggered mesh with spatial derivatives formulated using a second-order central finite-difference method. A third-order Runge–Kutta scheme is used for the nonlinear terms and a second-order implicit Crank–Nicholson scheme for the viscous terms in the temporal discretization. These are combined with the fractional-step method to enforce the continuity constraint. In this method, each time advancement consists of three steps and in each step, the discretized equations are first solved for an intermediate non-solenoidal velocity field without considering the continuity constraint (sub-step a). The Poisson equation is then solved for a virtual pressure field (sub-step b) which is subsequently used to project the velocity field onto a solenoidal velocity field (sub-steps c,d). These are detailed below for time step $n+1$:

step 1

$$\hat{u}_i = u_i^n + \Delta t\left(\gamma_1 H_i^n + \zeta_1 H_i^{n-1} + \frac{\alpha_1}{2Re}L_{jj}(\hat{u}_i + u_i^n) - \alpha_1(G_i(p'^n) + S_i^n)\right), \quad \text{(A 1}a\text{)}$$

$$L_{jj}(\phi^a) = \frac{1}{\alpha_1 \Delta t}D_i(\hat{u}_i), \quad \text{(A 1}b\text{)}$$

$$\frac{u_i^a - \hat{u}_i}{\Delta t} = -\alpha_1 G_i(\phi^a), \quad \text{(A 1}c\text{)}$$

$$p^a = p^n + \phi^a - \frac{\alpha_1 \Delta t}{2Re}L_{jj}(\phi^a); \quad \text{(A 1}d\text{)}$$

step 2

$$\hat{\hat{u}}_i = u_i^a + \Delta t\left(\gamma_2 H_i^a + \zeta_2 H_i^n + \frac{\alpha_2}{2Re}L_{jj}(\hat{\hat{u}}_i + u_i^a) - \alpha_2(G_i(p'^a) + S_i^a)\right), \quad \text{(A 2}a\text{)}$$

$$L_{jj}(\phi^b) = \frac{1}{\alpha_2 \Delta t}D_i(\hat{\hat{u}}_i), \quad \text{(A 2}b\text{)}$$

https://doi.org/10.1017/jfm.2012.498 Published online by Cambridge University Press

$$\frac{u_i^b - \hat{\hat{u}}_i}{\Delta t} = -\alpha_2 G_i(\phi^b), \tag{A 2c}$$

$$p^b = p^a + \phi^b - \frac{\alpha_2 \Delta t}{2Re} L_{jj}(\phi^b); \tag{A 2d}$$

step 3

$$\hat{\hat{\hat{u}}}_i = u_i^b + \Delta t \left(\gamma_3 H_i^b + \zeta_3 H_i^a + \frac{\alpha_3}{2Re} L_{jj}(\hat{\hat{\hat{u}}}_i + u_i^b) - \alpha_3 (G_i(p'^b) + S_i^b) \right), \tag{A 3a}$$

$$L_{jj}(\phi^{n+1}) = \frac{1}{\alpha_3 \Delta t} D_i(\hat{\hat{\hat{u}}}_i), \tag{A 3b}$$

$$\frac{u_i^{n+1} - \hat{\hat{\hat{u}}}_i}{\Delta t} = -\alpha_3 G_i(\phi^{n+1}), \tag{A 3c}$$

$$p^{n+1} = p^b + \phi^{n+1} - \frac{\alpha_3 \Delta t}{2Re} L_{jj}(\phi^{n+1}), \tag{A 3d}$$

where $i = 1, 2, 3$ stands for the three directions, the $H_i(=u_j \delta u_i / \delta x_j)$ are the discretized nonlinear terms, $D_i(=\delta/\delta x_i)$ is the divergence operator, $L_{jj}(=\delta^2/\delta x_1^2 + \delta^2/\delta x_2^2 + \delta^2/\delta x_3^2)$ is the Laplace operator, ϕ is the pressure corrections used to obtain the solenoidal velocity and pressure, and Δt is the time step. The pressure gradient is split into two components: S_i the mean pressure gradient applied to maintain the mass flow, and $G_i(p')(=\delta p'/\delta x_i)$ the fluctuation pressure gradient. A constant-mass-flow condition (as opposed to constant wall shear) is used in the simulations presented herein. In this method, the S_i in the spanwise and wall-normal directions are zero, but the streamwise component is set to the volume integration of the streamwise momentum equation at each step in a steady flow to ensure the mass flow rate is constant. In an unsteady flow simulation, the prescribed acceleration (in this case a constant value) is added to the streamwise mean pressure gradient during the accelerating period. The coefficients used in the above equations are (Orlandi 2001)

$$\gamma_1 = \tfrac{8}{15}, \quad \zeta_1 = 0, \quad \alpha_1 = \gamma_1 + \zeta_1 = \tfrac{8}{15}; \tag{A 4a}$$

$$\gamma_2 = \tfrac{5}{12}, \quad \zeta_2 = -\tfrac{17}{60}, \quad \alpha_2 = \gamma_2 + \zeta_2 = \tfrac{2}{15}; \tag{A 4b}$$

$$\gamma_3 = \tfrac{3}{4}, \quad \zeta_3 = -\tfrac{5}{12}, \quad \alpha_3 = \gamma_3 + \zeta_3 = \tfrac{1}{3}, \tag{A 4c}$$

and $\alpha_1 + \alpha_2 + \alpha_3 = 1$.

The Poisson equations in (A 1)–(A 3) are solved using an efficient two-dimensional fast Fourier transform (Orlandi 2001). In addition, owing to the use of an implicit scheme for the viscous terms, the calculation of the velocity fields $(\hat{u}, \hat{\hat{u}}, \hat{\hat{\hat{u}}},)$ requires the solution of equations involving a sparse matrix. Taking step 1 for example and rearranging (A 1*a*) gives

$$\left[1 - \frac{\alpha_1 \Delta t}{2Re} \left(\frac{\delta^2}{\delta x_1^2} + \frac{\delta^2}{\delta x_2^2} + \frac{\delta^2}{\delta x_3^2} \right) \right] \Delta u_i = RHS_i \tag{A 5}$$

where $\Delta u_i = \hat{u}_i - u_i^n$ with u_i^n being the component of the velocity in the i-direction at the nth sub-step, $\hat{u}_i$ the new intermediate non-solenoidal velocity and RHS_i is defined as

$$RHS_i = \Delta t \left[\gamma_1 H_i^n + \zeta_1 H_i^{n-1} - \alpha_1 (G_i(p'^n) + S_i^n) + \frac{\alpha_1}{Re} L_{jj}(u_i^n) \right]. \tag{A 6}$$

https://doi.org/10.1017/jfm.2012.498 Published online by Cambridge University Press

To solve this large sparse matrix, the splitting or factorization approximation is used (Orlandi 2001), in which the multi-dimensional problem is approximated by splitting it into a series of one-dimensional problems. Using the factorization technique and defining $A_{ij} = (\alpha_1 \Delta t/2Re)\,(\delta^2/\delta x_j^2)^i$, (A 5) is approximated by

$$(1 - A_{i1})(1 - A_{i2})(1 - A_{i3})\Delta u_i = RHS_i. \tag{A 7}$$

This approximation causes errors that are of the order of $O(\Delta t^2, \Delta x^2, \Delta y^2, \Delta z^2)$ which are the same as the errors already incurred in the space and time discretization. Equation (A 7) can now be solved in steps using a tri-diagonal matrix solver as follows:

$$(1 - A_{i1}) \quad \Delta u_i^{**} = RHS_i, \tag{A 8a}$$

$$(1 - A_{i3}) \quad \Delta u_i^{*} = \Delta u_i^{**}, \tag{A 8b}$$

$$(1 - A_{i2}) \quad \Delta u_i = \Delta u_i^{*}, \tag{A 8c}$$

where Δu^{**} and Δu^{*} are intermediate quantities with no physical significance, noting that the non-uniform wall-normal direction is solved last for convenience in varying the wall boundary conditions when necessary. Finally, the MPI is used to parallelize the code for use on a distributed-memory computer cluster.

REFERENCES

ABE, H., KAWAMURA, H. & MATSUO, Y. 2001 Direct numerical simulation of a fully developed turbulent channel flow with respect to the Reynolds number dependence. *Trans. ASME: J. Fluids Engng* **123** (2), 382–393 (also refer to the benchmark data website: http://murasun.me.noda.tus.ac.jp/turbulence/).

ANDERSSON, P., BERGGREN, M. & HENNINGSON, D. S. 1999 Optimal disturbances and bypass transition in boundary layers. *Phys. Fluids* **11** (1), 134–150.

ASAI, M., MINAGAWA, M. & NISHIOKA, M. 2002 The instability and breakdown of a near-wall low-speed streak. *J. Fluid Mech.* **455**, 289–314.

AVILA, K., MOXEY, D., DE LOZAR, A., AVILA, M., BARKLEY, D. & HOF, B. 2011 The onset of turbulence in pipe flow. *Science* **333** (6039), 192–196.

BRANDT, L., SCHLATTER, P. & HENNINGSON, D. S. 2004 Transition in boundary layers subject to free-stream turbulence. *J. Fluid Mech.* **517**, 167–198.

CARLSON, D. R., WINDALL, S. E. & PEETERS, M. F. 1982 Flow visualization study of transition in plane Poiseuille flow. *J. Fluid Mech.* **V 121**, 487–505.

CHUNG, Y. M. 2005 Unsteady turbulent flow with sudden pressure gradient changes. *Intl J. Numer. Meth. Fluids* **47** (8–9), 925–930.

COLOMBO, A. F., LEE, P. & KARNEY, B. W. 2009 A selective literature review of transient-based leak detection methods. *J. Hydro-environment Res.* **2** (4), 212–227.

DURBIN, P. & WU, X. 2007 Transition beneath vortical disturbances. *Annu. Rev. Fluid Mech.* **39**, 107–128.

ECKHARDT, B., SCHNEIDER, T. M., HOF, B. & WESTERWEEL, J. 2007 Turbulence transition in pipe flow. *Annu. Rev. Fluid Mech.* **39**, 447–468.

ELSNAB, J., KLEWICKI, J., MAYNES, D. & AMEEL, T. 2011 Mean dynamics of transitional channel flow. *J. Fluid Mech.* **678**, 451–481.

FORNARELLI, F. & VITTORI, G. 2009 Oscillatory boundary layer close to a rough wall. *Eur. J. Mech.* (B/*Fluids*) **28** (2), 283–295.

FRANSSON, J. H. M., MATSUBARA, M. & ALFREDSSON, P. H. 2005 Transition induced by free stream turbulence. *J. Fluid Mech.* **527**, 1–25.

https://doi.org/10.1017/jfm.2012.498 Published online by Cambridge University Press

GREENBLATT, D. & MOSS, E. A. 2004 Rapid temporal acceleration of a turbulent pipe flow. *J. Fluid Mech.* **514**, 65–75.

HE, S., ARIYARATNE, C. & VARDY, A. E. 2011 Wall shear stress in accelerating turbulent pipe flow. *J. Fluid Mech.* **685**, 440–460.

HE, S. & JACKSON, J. D. 2000 A study of turbulence under conditions of transient flow in a pipe. *J. Fluid Mech.* **408**, 1–38.

HE, S. & JACKSON, J. D. 2009 An experimental study of pulsating turbulent flow in a pipe. *Eur. J. Mech. (*B/*Fluids*) **28** (2), 309–320.

HERNON, D. O. M. H., WALSH, E. J. & MCELIGOT, D. M. 2007 Experimental investigation into the routes to bypass transition and the shear-sheltering phenomenon. *J. Fluid Mech.* **591**, 461–479.

JACOBS, R. G. & DURBIN, P. A. 2001 Simulations of bypass transition. *J. Fluid Mech.* **428**, 185–212.

JEONG, J. & HUSSAIN, F. 1995 On the identification of a vortex. *J. Fluid Mech.* **285**, 69–94.

KIM, J. & MOIN, P. 1985 Application of a fractional-step method to incompressible Navier–Stokes equations. *J. Comput. Phys.* **59** (2), 308–323.

KIM, J., MOIN, P. & MOSER, R. 1987 Turbulence statistics in fully developed channel flow at low Reynolds number. *J. Fluid Mech.* **177**, 133–166.

KLEBANOFF, P. S. 1971 Effect of free stream turbulence on the laminar boundary layer. *Bull. Am. Phys. Soc.* **10** (11), 1323.

LAGHA, M. 2007 Turbulent spots and waves in a model for plane Poiseuille flow. *Phys. Fluids* **19** (124103).

LUCHINI, P. 2000 Reynolds-number-independent instability of the boundary layer over a flat surface: optimal perturbations. *J. Fluid Mech.* **404**, 289–309.

MANDAL, A. C., VENKATAKRISHNAN, L. & DEY, J. 2010 A study on boundary-layer transition induced by free stream turbulence. *J. Fluid Mech.* **660**, 114–146.

MARUYAMA, T., KURIBAYASHI, T. & MIZUSHINA, T. 1976 The structure of the turbulence in transient pipe flows. *J. Chem. Engng Japan* **9** (6), 431–439.

MATSUBARA, M. & ALFREDSSON, P. H. 2001 Disturbance growth in boundary layers subjected to free stream turbulence. *J. Fluid Mech.* **430**, 149–168.

MELLIBOVSKY, F., MESEGUER, A., SCHNEIDER, T. M. & ECKHARDT, B. 2009 Transition in localized pipe flow turbulence. *Phys. Rev. Lett.* **103** (054502).

MESEGUER, Ã. & TREFETHEN, L. N. 2003 Linearized pipe flow to Reynolds number 107. *J. Comput. Phys.* **186** (1), 178–197.

MOIN, P. & MAHESH, K. 1998 Direct numerical simulation: a tool in turbulence research. *Annu. Rev. Fluid Mech.* **30**, 539–578.

MOSER, R. D., KIM, J. & MANSOUR, N. N. 1999 Direct numerical simulation of turbulent channel flow up to $Re_\tau = 590$. *Phys. Fluids* **11** (4), 943–945.

MULLIN, T. 2011 Experimental studies of transition to turbulence in a pipe. *Annu. Rev. Fluid Mech.* **43**, 1–24.

NAGARAJAN, S., LELE, S. K. & FERZIGER, J. H. 2007 Leading-edge effects in bypass transition. *J. Fluid Mech.* **572**, 471–504.

NOLAN, K. P., WALSH, E. J. & MCELIGOT, D. M. 2010 Quadrant analysis of a transitional boundary layer subject to free-stream turbulence. *J. Fluid Mech.* **658**, 310–335.

ORLANDI, P. 2001 *Fluid Flow Phenomena: A Numerical Toolkit*. Kluwer.

ORSZAG, S. A. 1971 Accurate solution of the Orr–Sommerfeld stability equation. *J. Fluid Mech.* **50** (4), 689–703.

OVCHINNIKOV, V., CHOUDHARI, M. M. & PIOMELLI, U. 2008 Numerical simulations of boundary-layer bypass transition due to high-amplitude free-stream turbulence. *J. Fluid Mech.* **613**, 135–169.

PFENNINGER, W. 1961 *Boundary Layer Suction Experiments with Laminar Flow at High Reynolds Numbers in the Inlet Length of a Tube by Various Suction Methods, in Boundary Layer and Flow Control* (ed. G. V. Lachmann), pp. 961–980. Pergamon.

RAI, M. M. & MOIN, P. 1993 Direct numerical simulation of transition and turbulence in a spatially evolving boundary layer. *J. Comput. Phys.* **109** (2), 169–192.

https://doi.org/10.1017/jfm.2012.498 Published online by Cambridge University Press

REYNOLDS, O. 1883 An experimental investigation of the circumstances which determine whether the motion of water shall be direct or sinuous and the law of resistance in parallel channels. *Phil. Trans. R. Soc. Lond.* **174**, 935–982.

RICCO, P., LUO, J. & WU, X. 2011 Evolution and instability of unsteady nonlinear streaks generated by free-stream vortical disturbances. *J. Fluid Mech.* **677**, 1–38.

ROACH, P. E. & BRIERLEY, D. H. 1992 The influence of a turbulent free stream on zero pressure gradient transitional boundary layer development part I: test cases T3A and T3B. In *Numerical Simulation of Unsteady Flows and Transition to Turbulence* (ed. O. Pironneau, W. Rodi, A. M. Rhyming, L. Savill & T. V. Truong), pp. 319–347. Cambridge University Press.

SCHLATTER, P., BRANDT, L., DE LANGE, H. C. & HENNINGSON, D. S. 2008 On streak breakdown in bypass transition. *Phys. Fluids* **20** (101505).

SCHUMACHER, J. & ECKHARDT, B. 2001 Evolution of turbulent spots in a parallel shear flow. *Phys. Rev.* E **63** (4 II), 463071–463079.

SCOTTI, A. & PIOMELLI, U. 2001 Numerical simulation of pulsating turbulent channel flow. *Phys. Fluids* **13** (5), 1367–1384.

SEDDIGHI, M. 2011 Study of turbulence and wall shear stress in unsteady flow over smooth and rough wall surfaces. PhD thesis, University of Aberdeen.

SEDDIGHI, M., HE, S., ORLANDI, P. & VARDY, A. E. 2011 A comparative study of turbulence in ramp-up and ramp-down unsteady flows. *Flow Turbul. Combust.* **86** (3–4), 439–454.

SHAN, H., MA, B., ZHANG, Z. & NIEUWSTADT, F. T. M. 1999 Direct numerical simulation of a puff and a slug in transitional cylindrical pipe flow. *J. Fluid Mech.* **387**, 39–60.

TARDU, S. F. & DA COSTA, P. 2005 Experiments and modeling of an unsteady turbulent channel flow. *AIAA J.* **43** (1), 140–148.

VAN, D. A., O'DONOGHUE, T., DAVIES, A. G. & RIBBERINK, J. S. 2011 Experimental study of the turbulent boundary layer in acceleration-skewed oscillatory flow. *J. Fluid Mech.* **684**, 251–283.

VAUGHAN, N. J. & ZAKI, T. A. 2011 Stability of zero-pressure-gradient boundary layer distorted by unsteady Klebanoff streaks. *J. Fluid Mech.* **681**, 116–153.

VOKE, P. R. & YANG, Z. 1995 Numerical study of bypass transition. *Phys. Fluids* **7** (9), 2256–2264.

WILLIS, A. P., PEIXINHO, J., KERSWELL, R. R. & MULLIN, T. 1876 Experimental and theoretical progress in pipe flow transition. *Phil. Trans. R. Soc. Lond.* A **366**, 2671–2684.

WU, X., JACOBS, R. G., HUNT, J. C. R. & DURBIN, P. A. 1999 Simulation of boundary layer transition induced by periodically passing wakes. *J. Fluid Mech.* **398**, 109–153.

WU, X. & MOIN, P. 2009 Direct numerical simulation of turbulence in a nominally zero-pressure-gradient flat-plate boundary layer. *J. Fluid Mech.* **630**, 5–41.

WYGNANSKI, I. J. & CHAMPAGNE, F. H. 1973 On transition in a pipe. Part 1. The origin of puffs and slugs and the flow in a turbulent slug. *J. Fluid Mech.* **59**, 281–335.

ZAKI, T. A. & DURBIN, P. A. 2005 Mode interaction and the bypass route to transition. *J. Fluid Mech.* **531**, 85–111.

ZAKI, T. A. & DURBIN, P. A. 2006 Continuous mode transition and the effects of pressure gradient. *J. Fluid Mech.* **563**, 357–388.

ZAKI, T. A. & SAHA, S. 2009 On shear sheltering and the structure of vortical modes in single- and two-fluid boundary layers. *J. Fluid Mech.* **626**, 111–147.

ZANG, T. A. & KRIST, S. E. 1989 Numerical experiments on stability and transition in plane channel flow. *Theor. Comput. Fluid Dyn.* **1** (1), 41–64.

https://doi.org/10.1017/jfm.2012.498 Published online by Cambridge University Press